



UNIVERSITÀ POLITECNICA DELLE MARCHE
Repository ISTITUZIONALE

Modeling and nonlinear dynamics of thermomechanically coupled composite plates

This is the peer reviewed version of the following article:

Original

Modeling and nonlinear dynamics of thermomechanically coupled composite plates / Rega, G.; Saetta, E.; Settini, V. - In: INTERNATIONAL JOURNAL OF MECHANICAL SCIENCES. - ISSN 0020-7403. - ELETTRONICO. - 187:(2020). [10.1016/j.ijmecsci.2020.106106]

Availability:

This version is available at: 11566/290324 since: 2024-04-28T12:58:34Z

Publisher:

Published

DOI:10.1016/j.ijmecsci.2020.106106

Terms of use:

The terms and conditions for the reuse of this version of the manuscript are specified in the publishing policy. The use of copyrighted works requires the consent of the rights' holder (author or publisher). Works made available under a Creative Commons license or a Publisher's custom-made license can be used according to the terms and conditions contained therein. See editor's website for further information and terms and conditions.

This item was downloaded from IRIS Università Politecnica delle Marche (<https://iris.univpm.it>). When citing, please refer to the published version.

note finali coverpage

(Article begins on next page)

This is a post-peer-review, pre-copyedit version of the paper

Modeling and nonlinear dynamics of thermomechanically coupled composite plates

by Giuseppe Rega^{1*}, Eduardo Saetta¹, Valeria Settimi¹

¹*Department of Structural and Geotechnical Engineering, Sapienza University of Rome, Italy*

*Corresponding author: giuseppe.rega@uniroma1.it

Please cite this work as follows:

Rega, G., Saetta, E., Settimi, V., Modeling and nonlinear dynamics of thermomechanically coupled composite plates, *International Journal of Mechanical Sciences*, **187**, 106106, 2020, DOI: 10.1016/j.ijmecsci.2020.106106.

Publisher link and Copyright information:

You can download the final authenticated version of the paper and the supplementary material from:
<https://doi.org/10.1016/j.ijmecsci.2020.106106>.
© 2020 Elsevier Ltd. All rights reserved.



This work is licensed under the Creative Commons Attribution-NonCommercial-NoDerivatives 4.0 International License. To view a copy of this license, visit <http://creativecommons.org/licenses/by-nc-nd/4.0/> or send a letter to Creative Commons, PO Box 1866, Mountain View, CA 94042, USA.

MODELING AND NONLINEAR DYNAMICS OF THERMOMECHANICALLY COUPLED COMPOSITE PLATES

Giuseppe Rega, Eduardo Saetta and Valeria Settimi

Department of Structural and Geotechnical Engineering, Sapienza University of Rome, Rome, Italy

Contents

- 1. Introduction**
- 2. A unified framework for 2D/0D multiphysics modeling**
- 3. Nonlinear models of thermomechanically coupled laminated plate**
 - 3.1 Two-dimensional modeling*
 - 3.2 Zero-dimensional modeling*
- 4. Validation of minimal ROMs**
 - 4.1 Linear dynamics and buckling*
 - 4.2 3D spatiotemporal thermal dynamics*
- 5. Nonlinear dynamics of TTC model**
 - 5.1 Dynamic buckling/post-buckling: a local and global analysis*
- 6. Effect of thermomechanical coupling**
- 7. Conclusions**

Highlights

- Thermomechanically coupled models constructed through a unified 2D formulation
- Minimal ROMs obtained and a reach yet cheap one selected for nonlinear dynamics
- Local and global dynamics analyzed for various boundary/body thermal excitations
- Complex interactions phenomena in slow-fast dynamics unveiled via global analysis
- Thermomechanical coupling effects addressed along with possible further reductions

Abstract

An overview of extended research recently pursued on unified continuous/reduced-order modeling and nonlinear dynamics of thermomechanical composite plates of interest in aerospace, mechanical and civil engineering is presented. Reduced models exhibit the fundamental features of geometrical nonlinearity and thermomechanical coupling of the underlying continua. The role of multiphysics coupling and the main features of nonlinear response obtained with variably refined minimal models is highlighted. Besides transverse mechanical excitation and mechanically or thermally-induced buckling, a variety of active thermal excitations, of body or boundary nature, are considered. Features of thermal response obtained with variably refined thermal assumptions are compared, in view of detecting cheap, yet reliable, models to be used for systematic numerical investigations. The effects of two-way thermomechanical coupling on local and global nonlinear dynamics are addressed through bifurcation diagrams, phase portraits and planar cross sections of 4D basins of attraction, highlighting the important role played by the slow transient thermal dynamics solely detectable with coupled models in the steady outcome of the swifter mechanical response. Conditions allowing to utilize partially coupled models or even the uncoupled mechanical one with prescribed steady temperature are discussed.

Keywords: Unified thermomechanical formulation, Composite plates, Continuous modeling, Reduced order models, Local and global nonlinear dynamics, Thermomechanical response, Two-/one-way coupling

1. Introduction

In connection with the increased importance of multiphysics phenomena in a variety of technological contexts, thermomechanical coupling of materials and structures in a nonlinear dynamics environment is a topic of major interest in aerospace engineering, but also in civil and mechanical engineering, as well as in micro-electro-mechanics. Two main alternative formulations of the coupled problem can be pursued, namely (i) one-way (i.e., partial) coupling, or (ii) two-way (i.e., full) coupling, although with several possible subcases.

The *one-way coupling* approach (from *thermal* to *mechanical*) relies on the reasonable assumption that thermal dynamics evolves over a much slower time-scale than mechanical dynamics, so that the former affects the latter but not vice versa. This means that changes in the mechanical response are produced by a thermal environment due to the presence of temperature-dependent coupling terms in the equations of motion, but no thermal effects are entailed by the structural motion. In this framework, the coupled problem is solved via two main sequential steps:

- (i) assuming the temperature distribution, or calculating it by solving the Fourier heat conduction equation;
- (ii) solving the mechanical equations, possibly with known temperature gradients.

Actually, in the case of slowly time-varying thermal environment, structural dynamics equations are usually modeled with a reference average temperature over a given structural time span. In the dimension reduction perspective, reduced order models (ROMs) based on vibration modes of the unheated structure (so called cold modes) are constructed, possibly complementing them with selected dual modes suitable to better capture the behavior of heated structures [1], or enhancing the reliability of a reference reduced basis through the interpolation among bases holding for different temperatures [2]. A slow temperature variation is essential to justify model reduction using an adaptive reduction basis, a procedure that does not work well when the temperature varies on a time-scale comparable to that of structural dynamics, as recently discussed by Jain and Tiso [3]. These authors have proposed a multiple time scales-based approach to solve the temperature-dependent structural dynamics equations by accounting for the coexisting slow/fast thermo/mechanical settings, highlighting the possibility to consistently reduce the equations of motion using a basis that slowly adapts to the instantaneous temperature configuration of the structure.

In the *two-way coupling* approach (from *thermal* to *mechanical*, and from *mechanical* to *thermal*), the thermal energy equation is coupled with the governing mechanical equations via the presence of additional mechanical (strain-rate or velocity) terms, which may be important for catching meaningful effects at both material and structure levels, even in a slowly varying temperature environment.

In this case, analysis is pursued:

- (i) taking the actual thermomechanical interaction into account;
- (ii) dealing at one time with temperature and displacement primary variables.

Within this framework, meaningful coupling effects have been highlighted in elastic materials under quasi-static thermal-mechanical loading since Nowinski [4], along with the dynamic effects caused by impact loading in inelastic monolithic materials [5-8]. More recently, dynamic effects in thermo-elastic-viscoplastic composites have been addressed via a three-dimensional (3D) multiscale approach [9] which combines global structural analysis with the generalized method of cells micromechanics theory [10]. For composite elastic beams and plates, actual thermomechanical coupling under quasi-static or dynamic loading has been considered in several investigations conducted via numerical approaches, including finite elements [11,12] and the Carrera Unified Formulation [13,14]. However, aerothermoelasticity is the nearly sole field (also including fluid coupling) where the importance of considering two-way dynamic coupling, in certain conditions, in the analysis of nonlinear problems (e.g., flutter) of hypersonic vehicles has been highlighted, instead of the typically used one-way approach which neglects the mutual coupling between elastic deformation and aerodynamic heating [15,16]. This is a matter that also required the development of simplified coupling procedures aimed at reducing the computational effort of comprehensive analyses. Analytical techniques have been utilized, too, a recent one focusing on the role that impedance metrics can play to characterize the

influence of two-way thermomechanical coupling on the nonlinear dynamics of a thermally buckled, harmonically excited beam, with also experimental verification, and to forecast extreme dynamics of structures operating in combined thermal and mechanical loading environments [17]. In the context of a modeling approach accounting for coupling of deformation and temperature fields in the nonlinear dynamics of structural members, and using Bubnov-Galerkin and finite difference methods [18], it is also worth mentioning a recent study of a plate-beam system for MEMS devices [19], although coupling was neglected in the quasi-static formulation considered as numerical experiment.

Focusing on the *nonlinear dynamics* of *plates* in a steady thermal environment, since the early review paper by Lee [20] one-way thermomechanical coupling has been assumed to analyze the influence of temperature on typical features of the nonlinear response, using both multi-degree-of-freedom (multi-dof) models and ROMs. Shi et al [21] analyzed the nonlinear thermal post-buckling of thin composite plates through a finite element formulation in modal coordinates making use of linear buckling mode shapes. Ribeiro [22] investigated the nonlinear vibrations of elastic and isotropic plates via a p -version, hierarchical, first-order shear deformation finite element, highlighting transitions from periodic to non-periodic motions when varying the temperature and the amplitude of transverse mechanical excitation.

Multi-dof models obtained by an energy approach have been considered in a number of works dealing with nonlinear vibrations and/or post-buckling of rectangular plates in thermal environments, using continuation and bifurcation analysis of the Lagrange-based ordinary differential equations (ODEs), also with experimental verifications. Considering fixed edges, Amabili and Carra [23] analyzed the influence of geometrical imperfections on the hardening/softening features of frequency-response curves of isotropic von Kármán plates, whereas Amabili and Tajahmadi [24] addressed the temperature effects on post-buckling displacements of laminated and isotropic plates with higher order shear deformation. Alijani et al [25] used bifurcation diagrams of Poincaré maps and maximum Lyapunov exponent to detect and classify bifurcations and complex nonlinear dynamics in a multi-dof model with quadratic and cubic nonlinearities of simply supported FGM plates with movable edges, using von Kármán and first-order shear deformation theories.

Nonlinear oscillations, bifurcations and chaos of FGM plates in a thermal environment (uniform over the plate surface and variable along the thickness) have been dealt with also via ROMs obtained by discretizing the underlying partial differential equations (PDEs), considering temperature-dependent material properties. Using Reddy's higher-order shear deformation theory and an improved perturbation technique, Huang and Shen [26] investigated the nonlinear fundamental frequency and vibration characteristics of a single-dof model, showing that the temperature field has a significant effect on the plate nonlinear vibration and dynamic response. Yuda and Zhiqiang [27] investigated numerically bifurcation and chaos phenomena in a circular plate under one- and two-term transversal excitations in thermal environment via a Duffing type equation, highlighting the existence of chaos with the Melnikov method. Based on third-order shear deformation theory, Galerkin discretization of PDEs and numerical simulation of the averaged equations provided by different asymptotic methods, periodic, quasiperiodic and chaotic motions were seen to occur, under certain conditions, in a 1:1 internally resonant two-dof model under parametric and external excitations [28], and in a three-dof model with 1:2:4 internal resonance and combined principal parametric and $1/2$ -subharmonic resonances [29].

Thermoelastic ROMs of an isotropic circular plate based on nonlinear Mindlin plate theory with one-dof and three-dof, have been used by Warminska et al [30] and Manoach et al [31], respectively. They analyzed the influence of a uniformly distributed (along plate span and thickness) temperature on the buckling and post-buckling regular and chaotic oscillations, on mode involvement in resonances, and on interactions coming from thermal and mechanical couplings, with also finite element validation in terms of natural frequency/modes and time simulation of transient analysis for selected parameter values.

However, in general, the case study-dependent nature and the computational costs of numerical investigations of finite amplitude vibrations of geometrically nonlinear structures with multi-dof models strongly limit the possibility to obtain fundamental insight into thermal-structural interactions via parametric studies. Thus, developing reliable ROMs for nonlinear dynamic analyses turns out to be even more important

when dealing with *two-way* thermomechanical coupling. Indeed, two-way coupled reduced models of plates employing single-term Galerkin expansions for both the transverse displacement and two thermally-induced stress resultants have been used to describe different phenomena. These include thermoelastic damping of the response, with the ensuing stabilizing effects [32-35], bifurcation and chaotic dynamics (the latter being characterized through fractal dimension and maximum Lyapunov exponent) in isotropic [34] and orthotropic [35] plates, the influence of various material parameters on the decay of nonlinear vibration amplitudes [36].

Overall, low-order models preserving the main features of the underlying continuum formulations get rid of the complicatedness generally occurring in the analysis and interpretation of nonlinear phenomena when using richer models (e.g., finite elements), also possibly implemented within an effective unified perspective [13,37,38]. Thus, they allow easier analyses and deeper understanding of the basic, yet involved, effects of coupling on the finite amplitude vibrations of geometrically nonlinear structures. These include, among others, the meaningful effects entailed by the *transient slow thermal* dynamics on the *steady fast mechanical* response recently highlighted for composite plates in both passive [39] and active thermal regime [40,41], and the influence of slowly changing thermal loads on the post-buckled and snap-through vibrations of beam-plate micro-electro-mechanical devices [17].

The present paper is framed in the nonlinear dynamics of thermomechanically coupled composite plates addressed via two-way coupled ROMs, and aims at providing an overview both of the continuum and reduced analytical formulations ending up to minimal models, and of some fundamental aspects of their dynamical response as obtained through a comprehensive nonlinear analysis. It is based on the modeling [42-45] and nonlinear dynamics [39-41,46] accomplishments in a number of recent papers that have allowed the authors to grasp some fundamental, yet varied and intriguing, nonlinear phenomena which characterize the response of thermomechanically coupled plates.

The topic will be addressed by identifying a number of objectives to be properly attained through a related sequence of analytical/numerical investigations.

1. Formulating the plate thermomechanical problem at the two-dimensional (2D) continuous level in a unified way, and developing a consistent and controllable dimension reduction aimed at identifying zero-dimensional (0D) minimal models suitable for computationally burdensome investigations of the relevant nonlinear/complex dynamics.
2. Characterizing and comparing ROMs in terms of functionality, flexibility, and cheapness, and validating models in terms of mechanical and thermal response.
3. Systematically analyzing nonlinear response of a class of composite plates with a ‘best’-selected minimal model via local and global dynamics tools, by considering a variety of thermal excitations in addition to mechanical ones; investigating transient and steady coupled response ensuing from the slow/fast evolution of thermal/mechanical variables, and evaluating the effects of thermomechanical coupling with also a view to possibly using solely one-way coupled models.

The paper is organized as follows. Section 2 presents a unified framework for 2D/0D multiphysics modeling. Nonlinear models of thermomechanically coupled laminated plates at both continuum and reduced order levels, respectively governed by PDEs and ODEs, are presented in Sect. 3. Within the dimension reduction perspective necessary to effectively deal with nonlinear dynamics problems, models validation in linear dynamics and buckling is presented in Sect. 4, along with the capability of underlying thermal assumptions to reliably describe variable response regimes. Section 5 summarizes some main outcomes of a systematic investigation of nonlinear dynamics as obtained with a quite refined reference model, by distinguishing between different cases of thermal excitation, which include boundary conditions and body sources. Section 6 investigates the influence of modeling refinements/simplifications on the extent and features of the highlighted thermomechanical coupling. A conclusions section ends the paper.

2. A unified framework for 2D/0D multiphysics modeling

Tonti's diagram [47,48] for the physical theories is used as a suitable framework to implement a unified, multiphysics, consistent and controllable formulation of the thermomechanical problem for geometrically nonlinear laminated plates undergoing finite amplitude vibrations. In its more general formulation, at either continuum (3D, 2D) or reduced-order (0D) level, such modeling framework based on Tonti diagram decomposes the fundamental equations of a generic multiphysics theory into three sets of equations, i.e. balance, configuration, and phenomenological (Fig. 1(a)). Each of the first two sets links with each other the fundamental variables (source and configuration, respectively) and some corresponding expressive variables, while the set of phenomenological equations establishes relations among variables of the balance and configuration sets.

In the 2D engineering multiphysics modeling of elastic plates, a similar diagram is obtained starting from the basic assumption $3D \rightarrow 2D$

$$\{3D \text{ configuration variables}\} = \{\text{shape}\} \times \{\text{generalized configuration variables (2D)}\}, \quad (1)$$

that expresses the 3D configuration variables in terms of 2D generalized ones through assumed mathematical function shapes, and correspondingly generalizing all equations and variables of Tonti's decomposition. Performing this procedure for the 2D modeling of nonlinear thermomechanical composite plates, the scheme in Fig. 1(b) is formulated, where mass force and source energy are fundamental balance variables, displacement and temperature are fundamental configuration variables, and the corresponding mechanical and thermal expressive variables are recognized, along with the schematic relations among variables in the balance, configuration and phenomenological sets of equations. A configuration approach (blue arrow in Fig. 1(b)) allows to obtain the fundamental plate model, namely the thermomechanical governing equations directly linking the fundamental balance and configuration variables, with the relevant boundary and initial conditions to be properly specified.

After introducing a basic reducing assumption similar to Eq. (1) and allowing to pass from generalized 2D configuration variables to correspondingly reduced zero-dimensional (0D) variables, Tonti-like diagrams for variably reduced models can be formulated, as it will be shown forward for sample minimal models to be possibly considered for nonlinear dynamics investigations.

3. Nonlinear models of thermomechanically coupled laminated plate

3.1 Two-dimensional modeling

Several nonlinear 2D models of thermomechanically coupled plates can be formulated according to a variety of underlying mechanical and thermal assumptions possibly introduced as regards the shape functions in Eq. (1), which allow to pass from the 3D to the 2D formulation. In the framework of plate structural theories combined with the equivalent single layer approach [49], plate deformation is described by the deformation of its reference midplane and the shear-warping of its cross-section, with approximations for the former and the latter leading to geometrically nonlinear and shear deformation theories, respectively. In turn, approximations for the temperature field distribution along the plate thickness and midplane lead to thermal equations.

The unified scheme of Fig. 1(b) allows to formulate and compare different continuous models with full thermoelastic coupling, which result from different assumptions about the plate mechanical and thermal configurations. The resulting models are not equally advantageous. As regards geometrical nonlinearities, *general* models accounting for all of them [50,51] involve significant computational difficulties when aiming to obtain minimal discretized models for the analysis of nonlinear vibrations through the procedure generally used for *classical* von Kármán models. On the other hand, von Kármán strains - although involving some nonlinear terms - do not account for the change of structural configuration within the curvature-displacement

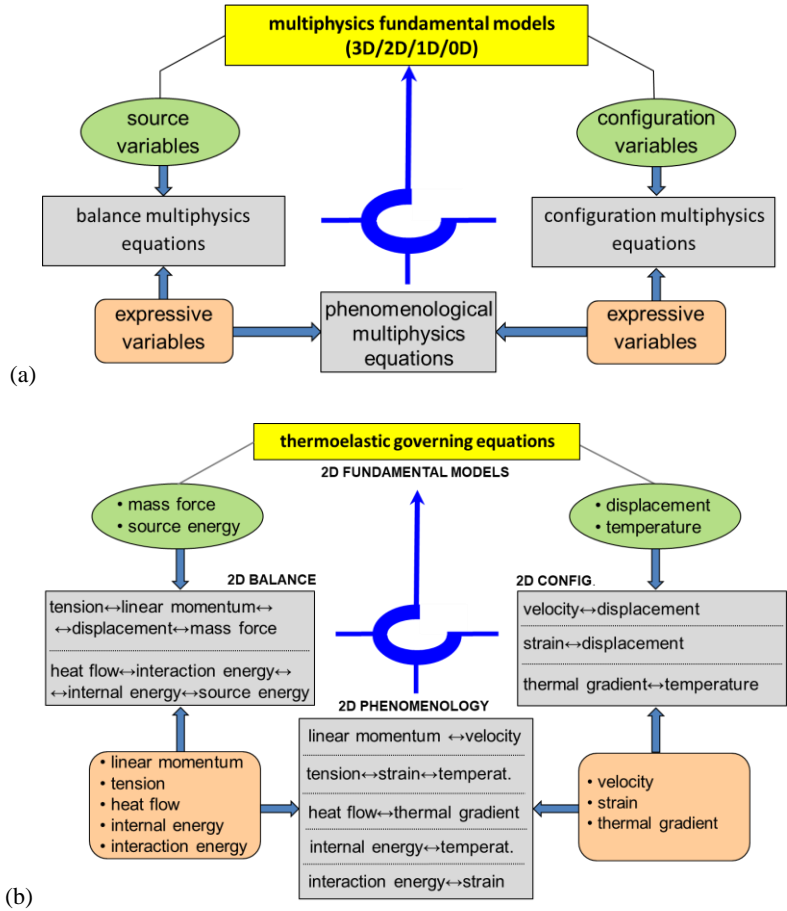


Fig. 1. (a) General multiphysics modeling framework based on Tonti diagram for physical theories; (b) unified scheme for thermomechanical 2D plate.

relationship, because of considering only linear terms in the curvature expressions. Yet, the neglected geometrical nonlinearities may entail non-negligible effects in the nonlinear analysis of composite plates.

Therefore, in addition to the general and von Kármán types of continuous models, *modified* models [52,53] also accounting for nonlinear terms in the curvature expressions can be considered. They retain the great advantage of all von Kármán models as regards performing minimal reductions. Based on a variety of kinematical and thermal features, Table 1 shows some possible models going from the most complete one on the left, which accounts for fully coupled deformation (GTTC, General Third-order theory with Thermomechanical Coupling), to the simplest one on the right accounting for Kirchoff-von Kármán deformation (CTC, Classical theory with Thermomechanical Coupling). Overall, as outlined above, they are classified as (i) general models, which turn out to be mathematically intractable in a reduced order modeling perspective based on kinematic condensation, (ii) classical von Kármán models, mathematically tractable for all types of laminates, and (iii) modified, i.e. intermediate, models, mathematically tractable only for symmetric laminates. Aiming to obtain minimal order models for different types of laminates, to be possibly tackled with asymptotic techniques besides numerical ones, in the following attention will be restricted to the TTC (Third-order theory with Thermomechanical Coupling) model, while also considering the CTC one for comparison purposes. Note that, from the mechanical viewpoint, the two models take into account (up to third-order) and neglect shear deformation, respectively, and, from the thermal viewpoint, they consistently assume a correspondingly cubic or linear variation of the unknown temperature field along the thickness.

Consider the laminated rectangular plate in Fig.2, with N layers, thickness h and edge lengths a and b in the x - and y -directions, respectively. The reference plane of the plate coincides with the xy plane of an orthogonal Cartesian coordinate system. The plate is subject to a time-varying, distributed, transverse mechanical excitation, and to a 3D thermal body source due to, e.g., passage of an electric current through the

Table 1. Some general, modified, and classical continuous models of composite plates.

Features	General		Modified		Classical (von Kármán deformation)		
	GTTC	GCTC	MGFTC	MGCTC	TTC	FTC	CTC
in-plane deformation	cubic	cubic	quadratic	quadratic	quadratic	quadratic	quadratic
flexural and twisting curvatures	cubic	cubic	cubic	cubic	linear	linear	linear
spiral curvatures	quadratic	quadratic	absent	absent	absent	absent	absent
shear deformability	cubic	absent	linear	absent	cubic	linear	absent
temperature along the thickness	cubic	linear	linear	linear	cubic	linear	linear

plate, chemical reactions or nuclear fission [54], which is assumed to vary along the thickness with a constant (E^C) and a linear (E^L) contribution.

Moreover, the plate edges are subject to steady uniform stretching forces of magnitudes p_x and p_y in the x - and y -directions, respectively. Other mechanical and thermal conditions on the edges, and thermal boundary conditions on the plate upper and lower surfaces will be specified forward, along with the elastic and thermal properties of the material.

For the TTC model, the mechanical version of Eq. (1) reads:

$$u_1 = u + z\phi_1 - \frac{4}{3h^2}z^3(\phi_1 + w_{,x}), \quad u_2 = v + z\phi_2 - \frac{4}{3h^2}z^3(\phi_2 + w_{,y}), \quad u_3 = w \quad (2)$$

where $u_1(x, y, z, t)$, $u_2(x, y, z, t)$ and $u_3(x, y, z, t)$ are the components of the 3D displacement variable along the x , y and z directions, while $u(x, y, t)$, $v(x, y, t)$, $w(x, y, t)$ are the displacements of a point located on the midplane and $\phi_1(x, y, t)$, $\phi_2(x, y, t)$ are the rotations of a transverse normal about the y - and x -axes. The latter represent the unknown displacements (independent of z) of the 2D plate model.

In turn, the thermal version of Eq. (1) reads:

$$T = T_0 + zT_1 + z^2T_2 + z^3T_3 \quad (3)$$

where $T(x, y, z, t)$ is the 3D temperature field (to be intended as temperature increment with respect to the natural state of reference), while $T_0(x, y, t)$, $T_1(x, y, t)$, $T_2(x, y, t)$, $T_3(x, y, t)$ are the unknown components of the temperature in the 2D model (see Fig. 3(b) forward). The components T_2 and T_3 can be expressed in terms of T_0 and T_1 by imposing a variable (pure or mixed) combination of the following thermal boundary conditions on the plate upper and lower surfaces:

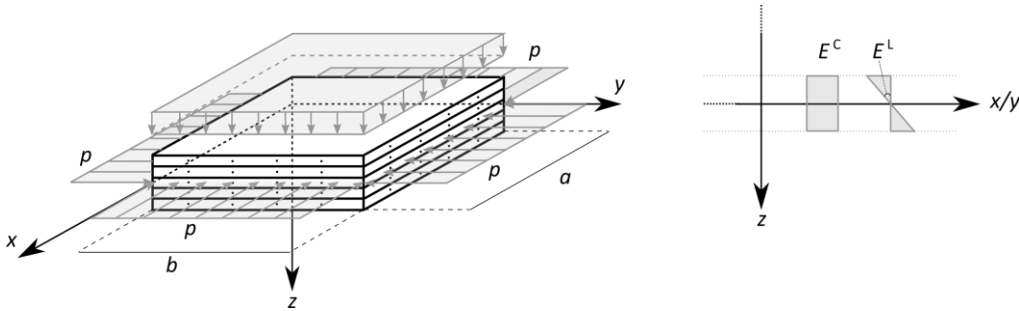


Fig. 2. Laminated plate under in-plane (p) and transverse mechanical loads, and body constant (E^C) and linear (E^L) thermal sources distributed along the thickness.

$$q_3|_{z=\pm h/2} = \pm H[T_\infty - (T)_{\pm h/2}] \quad \text{free heat exchange} \quad (4)$$

$$\frac{\partial T}{\partial z}\Big|_{z=\pm h/2} = 0 \quad \text{thermal insulation} \quad (5)$$

$$T|_{z=\pm h/2} = T^*(x, y, t) \quad \text{temperature prescribed} \quad (6)$$

$$q_3|_{z=\pm h/2} = q_3^*(x, y, t) \quad \text{heat flow prescribed} \quad (7)$$

where q_3 is the heat flow in z direction, H is the boundary conductance, T_∞ is the constant difference between the absolute temperature of the surrounding medium and the reference temperature, and T^* and q_3^* are the temperature and heat flow prescribed on the external surfaces, respectively. This results in a temperature cubic profile in terms of the sole unknown T_0 (membrane) and T_1 (bending) temperatures:

$$T = f_a(z)T_0 + f_b(z)T_1 + f_c(z) \quad (9)$$

where

$$\begin{aligned} f_a(z) &= (r_1 + r_2z + r_3z^2 + r_4z^3), & f_b(z) &= (r_5 + r_6z + r_7z^2 + r_8z^3), \\ f_c(z) &= (r_9 + r_{10}z + r_{11}z^2 + r_{12}z^3) \end{aligned} \quad (10)$$

with the coefficients r_i depending on the kind of imposed conditions.

For the CTC model, Eqs. (2) and (3) without the nonlinear z -terms hold, and Eq. (9) reduces to

$$T = T_0 + zT_1 \quad (11)$$

which allows to prescribe on the plate upper and lower surfaces only the boundary condition (4) of free heat exchange.

A summary of explicit variables/equations entering the unified scheme of Fig. 1(b) is reported in Figs. 3 and 4, with the yellow-marked parts to be intended as present (absent or given values) in the TTC (CTC) model. Specifically, Figure 3 lists the fundamental and expressive, mechanical and thermal, variables in the top and bottom light-brown stripes, respectively, with the configuration/balance equations linking them being reported in the middle. In Fig. 3(a), $\varepsilon_{ij}^{(0)}$ are von Kármán nonlinear membrane strains, $\varepsilon_{ij}^{(1)}$ Kirchhoff linear bending strains (curvatures), $\varepsilon_{ij}^{(3)}$ Reddy higher order bending strains, $\gamma_i^{(0)}$ Mindlin linear transverse shearing strains, and $\gamma_i^{(2)}$ Reddy higher order transverse shearing strains. In Fig. 3(c), $F_i^{(0)}$, ($i=1,2,3$), and $F_i^{(1)}$, ($i=1,2$), are 2D force and couple components of the 3D body forces $f_i(x, y, z, t)$, ($i=1,2,3$), along the x , y and z directions, N_{ij} are membrane forces, M_{ij} bending moments, P_{ij} higher order bending moments, Q_i transverse shearing forces, S_i higher order transverse shearing forces, R_i linear momentum variables. In Fig. 3(b), $g_i^{(0)}$ and $g_i^{(1)}$ are 2D membrane and bending thermal gradients, respectively. In Fig. 3(d), $E^{(0)}$ and $E^{(1)}$ are 2D membrane and bending thermal components of the 3D body source energy $E(x, y, z, t)$. In turn, Figure 4 lists the various kinds of phenomenological equations (purely monophysics or involving multiphysics coupling), suitably arranged.

Combining configuration, phenomenological and balance equations, the fundamental PDEs governing the 2D nonlinear dynamics of the thermomechanical laminated plate in terms of the corresponding *displacement* and *temperature* variables are obtained, for the TTC or CTC model. Even if truncating them to the third-order, the equations display nonlinear geometrical coupling among nearly all variables, and are very involved when a generic laminate is considered. Further analytical details can be found in [42,44].

(a) CONFIGURATION (mechanical)

displacement: $\{u \ v \ w \ \phi_1 \ \phi_2\}$

velocity↔displacement
 $u^v = u_{,t}; \ v^v = v_{,t}; \ w^v = w_{,t}; \ \phi_1^v = \phi_{1,t}; \ \phi_2^v = \phi_{2,t}$

strain↔displacement
 $\varepsilon_{11}^{(0)} = u_{,x} + \frac{1}{2} w_{,x}^2; \ \varepsilon_{22}^{(0)} = v_{,y} + \frac{1}{2} w_{,y}^2; \ \varepsilon_{12}^{(0)} = u_{,y} + v_{,x} + w_{,x} w_{,y}$
 (inplane strain↔displacement)

$\varepsilon_{11}^{(1)} = \phi_{1,x}; \ \varepsilon_{22}^{(1)} = \phi_{2,y}; \ \varepsilon_{12}^{(1)} = \phi_{1,y} + \phi_{2,x}$
 (curvature↔displacement)

$\gamma_2^{(0)} = \phi_2 + w_{,y}; \ \gamma_1^{(0)} = \phi_1 + w_{,x};$
 (transverse shear strain↔displacement)

$\varepsilon_{11}^{(3)} = -c_1 (\phi_{1,x} + w_{,xx}); \ \varepsilon_{22}^{(3)} = -c_1 (\phi_{2,y} + w_{,yy});$
 $\varepsilon_{12}^{(3)} = -c_1 (\phi_{1,y} + \phi_{2,x} + 2w_{,xy}); \quad (c_1 = 4/3h^2; \ c_2 = 3c_1)$
 $\gamma_2^{(2)} = -c_2 (\phi_2 + w_{,y}); \ \gamma_1^{(2)} = -c_2 (\phi_1 + w_{,x});$
 (higher order strain↔displacement)

velocity: $\{u^v \ | \ v^v \ | \ w^v \ | \ \phi_1^v \ | \ \phi_2^v\}$

strain: $\{\varepsilon_{ij}^{(0)} \ | \ \varepsilon_{ij}^{(1)} \ | \ \varepsilon_{ij}^{(3)} \ | \ \gamma_1^{(0)} \ | \ \gamma_2^{(0)} \ | \ \gamma_1^{(2)} \ | \ \gamma_2^{(2)}\}$

(b) CONFIGURATION (thermal)

temperature: $\{T_0 \ T_1\}$

$T = f_a(z)T_0 + f_b(z)T_1 + f_c(z)$ with f_a, f_b, f_c depending on the thermal boundary conditions on the external surfaces

thermal gradient↔temperature
 $g_1^{(0)} = T_{0,x}; \ g_2^{(0)} = T_{0,y};$ (in-plane thermal configuration)
 $g_1^{(1)} = T_{1,x}; \ g_2^{(1)} = T_{1,y};$ (out-of-plane thermal configuration)

thermal gradient: $\{g_1^{(0)} \ g_2^{(0)} \ | \ g_1^{(1)} \ g_2^{(1)}\}$

(c) BALANCE (mechanical)

mass force: $\{F_1^{(0)} \ F_2^{(0)} \ F_3^{(0)} \ F_4^{(1)} \ F_5^{(1)}\}$

tension↔ linear momentum ↔displacement↔mass force

$N_{11,x} + N_{12,y} - R_{1,t} + F_1^{(0)} = 0$ (mechanical balance along x)

$N_{12,x} + N_{22,y} - R_{2,t} + F_2^{(0)} = 0$ (mechanical balance along y)

$M_{11,xx} + 2M_{12,xy} + M_{22,yy} + (N_{11}w_{,x} + N_{12,y})_{,x} + (N_{12}w_{,x} + N_{22,y})_{,y} + R_{3,t} + F_3^{(0)} = 0$ (mechanical balance along z)

$(M_{11} - c_1 P_{11})_{,x} + (M_{12} - c_1 P_{12})_{,y} - Q_1 + c_2 S_1 - R_{4,t} + F_4^{(1)} = 0$ (mechanical balance around y)

$(M_{12} - c_1 P_{12})_{,x} + (M_{22} - c_1 P_{22})_{,y} - Q_2 + c_2 S_2 - R_{5,t} + F_5^{(1)} = 0$ (mechanical balance around y)

tension: $\{N_{11} \ N_{22} \ N_{12} \ | \ M_{11} \ M_{22} \ M_{12} \ | \ P_{11} \ P_{22} \ P_{12} \ | \ Q_1 \ Q_2 \ | \ S_1 \ S_2\}$

linear momentum: $\{R_1 \ R_2 \ R_3 \ | \ R_4 \ | \ R_5\}$

(d) BALANCE (thermal)

source energy: $\{E^{(0)} \ E^{(1)}\}$

heat flow↔interaction energy↔internal energy↔source e.

$q_{1x}^{(0)} + q_{2y}^{(0)} + Q^{(0)} - b_t^{(0)} - a_t^{(0)} = E^{(0)}$ (membrane-thermal balance)

$q_{1x}^{(1)} + q_{2y}^{(1)} + Q^{(1)} - b_t^{(1)} - a_t^{(1)} = E^{(1)}$ (bending-thermal balance)

$Q^{(0)}$: rates of energy related to transversal 3D heat q_3 flow (determined by the thermal boundary conditions)

heat flow: $\{q_1^{(0)} \ q_2^{(0)} \ | \ q_1^{(1)} \ q_2^{(1)}\}$

internal energy: $\{b^{(0)} \ | \ b^{(1)}\}$

interaction energy: $\{a^{(0)} \ | \ a^{(1)}\}$

Fig. 3. Particularization of configuration (a,b) and balance (c,d) equations of the unified scheme of Fig.1 for TTC and CTC (yellow-marked parts skipped) models: mechanical (a,c) and thermal (b,d), fundamental (green) and expressive (red) variables.

3.2 Zero-dimensional modeling

A zero-dimensional reduction of 2D continuous models is performed starting from the basic assumption:

$$\{\text{generalized configuration variables (2D)}\} = \{\text{shape}\} \times \{\text{reduced configuration variables (0D)}\}, \quad (12)$$

in which the 0D reduced configuration variables depend only on time t , while the shape functions govern the dependence on x and y in the plate reference plane.

For the TTC model, the general mathematical form of Eq. (12) reads:

$$u(x, y, t) = \sum_{m=1}^M \sum_{n=1}^N \psi_{mn}^u(x, y) U_{mn}(t); \quad v(x, y, t) = \sum_{m=1}^M \sum_{n=1}^N \psi_{mn}^v(x, y) V_{mn}(t); \quad (13a)$$

$$w(x, y, t) = \sum_{m=1}^M \sum_{n=1}^N \psi_{mn}^w(x, y) W_{mn}(t); \quad (13b)$$

$$\phi_1(x, y, t) = \sum_{m=1}^M \sum_{n=1}^N \psi_{mn}^{\phi_1}(x, y) \Phi_{1mn}(t); \quad \phi_2(x, y, t) = \sum_{m=1}^M \sum_{n=1}^N \psi_{mn}^{\phi_2}(x, y) \Phi_{2mn}(t); \quad (13c)$$

$$T_0(x, y, t) = \sum_{m=1}^M \sum_{n=1}^N \psi_{mn}^{T_0}(x, y) T_{R0mn}(t); \quad T_1(x, y, t) = \sum_{m=1}^M \sum_{n=1}^N \psi_{mn}^{T_1}(x, y) T_{R1mn}(t) \quad (13d)$$

where the generic sets of assumed shape functions ψ_{mn} must satisfy the mechanical and thermal boundary conditions on the plate edges, and the sets of unknown components for the reduced configuration variables read:

$$\text{reduced displacement:} \quad \{U_{mn} \quad V_{mn} \quad W_{mn} \quad \Phi_{1mn} \quad \Phi_{2mn}\} \quad (14a)$$

$$\text{reduced temperature:} \quad \{T_{R0mn} \quad T_{R1mn}\} \quad (14b)$$

In the context of a minimal Galerkin discretization, the seven 2D configuration variables $u, v, w, \phi_1, \phi_2, T_0, T_1$ may be expressed in terms of seven corresponding time-dependent reduced variables $U, V, W, \Phi_1, \Phi_2, T_{R0}, T_{R1}$ through only one shape function for each component. Accordingly, if using the TTC two-dimensional model, the minimal zero-dimensional ROM for a generic laminate will consist of seven temporal ODEs (five mechanical and two thermal) with seven corresponding unknowns. Instead, if using the shear-indeformable CTC model, the minimal ROM will have five ODEs (three mechanical and two thermal) with five corresponding unknowns.

It is worth noting that, for the TTC model, a dimensional reduction of the component thermal problem has been already performed at the 2D level, based on the sole assumption of cubic temperature distribution along the thickness, which has allowed to link the higher-order components T_2 and T_3 to the constant (T_0) and linear (T_1) ones via the thermal boundary conditions prescribed on the upper and lower surfaces. Under suitable assumptions and approximations, also the component mechanical problem can be further reduced via proper condensation procedures.

The first kinematic condensation is performed at the 2D level for both TTC and CTC models, and is concerned with transforming the formerly fundamental in-plane configuration variables u and v of the mechanical problem to slave variables, similar to what is usually carried out in the literature for the purely mechanical von Kármán model. This can be accomplished under the following conditions:

- no coupling terms containing u or v exist in the in-plane mechanical balance equations;
- the corresponding in-plane inertia forces are negligible ($I_0 \ddot{u} = I_0 \ddot{v} = 0$);
- the density of the plate is constant ($I_1 = 0$);
- the in-plane body forces are eliminated ($F_1^{(0)} = F_2^{(0)} = 0$).

Note that the second assumption corresponds to considering the frequencies of in-plane vibration much higher than the frequency of transverse vibration.

PHENOMENOLOGY

linear momentum ↔ velocity

$$R_1 = I_0 u^v + (I_1 - c_1 I_3) \phi_x^v - c_1 I_3 w_x^v, \quad R_2 = I_0 v^v + (I_1 - c_1 I_3) \phi_y^v - c_1 I_3 w_y^v, \quad R_4 = (I_1 - c_1 I_3) u^v + (I_2 - 2c_1 I_4 + c_1^2 I_6) \phi_x^v - c_1 (I_4 - c_1 I_6) w_x^v$$

$$R_3 = I_0 w^v - c_1^2 I_6 (w_{xx}^v + w_{yy}^v) + c_1 [I_5 (u_{xx}^v + v_{xx}^v) + (I_4 - c_1 I_6) (\phi_{1,x}^v + \phi_{2,y}^v)], \quad R_5 = (I_1 - c_1 I_3) v^v + (I_2 - 2c_1 I_4 + c_1^2 I_6) \phi_y^v - c_1 (I_4 - c_1 I_6) w_y^v$$

tension ↔ strain ↔ temperature

(membrane constitutive relation)

$$\begin{Bmatrix} N_{11} \\ N_{22} \\ N_{12} \end{Bmatrix} = \begin{bmatrix} A_{11} & A_{12} & A_{16} \\ A_{12} & A_{22} & A_{26} \\ A_{16} & A_{26} & A_{66} \end{bmatrix} \begin{Bmatrix} \epsilon_{11}^{(0)} \\ \epsilon_{22}^{(0)} \\ \epsilon_{12}^{(0)} \end{Bmatrix} + \begin{bmatrix} B_{11} & B_{12} & B_{16} \\ B_{12} & B_{22} & B_{26} \\ B_{16} & B_{26} & B_{66} \end{bmatrix} \begin{Bmatrix} \epsilon_{11}^{(1)} \\ \epsilon_{22}^{(1)} \\ \epsilon_{12}^{(1)} \end{Bmatrix} + \begin{bmatrix} E_{11} & E_{12} & E_{16} \\ E_{12} & E_{22} & E_{26} \\ E_{16} & E_{26} & E_{66} \end{bmatrix} \begin{Bmatrix} \epsilon_{11}^{(3)} \\ \epsilon_{22}^{(3)} \\ \epsilon_{12}^{(3)} \end{Bmatrix}$$

$$- \begin{bmatrix} r_1 \beta_{11}^A + r_2 \beta_{11}^B + r_3 \beta_{11}^D + r_4 \beta_{11}^E & r_5 \beta_{11}^A + r_6 \beta_{11}^B + r_7 \beta_{11}^D + r_8 \beta_{11}^E & r_9 \beta_{11}^A + r_{10} \beta_{11}^B + r_{11} \beta_{11}^D + r_{12} \beta_{11}^E \\ r_1 \beta_{22}^A + r_2 \beta_{22}^B + r_3 \beta_{22}^D + r_4 \beta_{22}^E & r_5 \beta_{22}^A + r_6 \beta_{22}^B + r_7 \beta_{22}^D + r_8 \beta_{22}^E & r_9 \beta_{22}^A + r_{10} \beta_{22}^B + r_{11} \beta_{22}^D + r_{12} \beta_{22}^E \\ r_1 \beta_{12}^A + r_2 \beta_{12}^B + r_3 \beta_{12}^D + r_4 \beta_{12}^E & r_5 \beta_{12}^A + r_6 \beta_{12}^B + r_7 \beta_{12}^D + r_8 \beta_{12}^E & r_9 \beta_{12}^A + r_{10} \beta_{12}^B + r_{11} \beta_{12}^D + r_{12} \beta_{12}^E \end{bmatrix} \begin{Bmatrix} T_0 \\ T_1 \end{Bmatrix}$$

($r_1 = r_6 = 1$)

(bending constitutive relation)

$$\begin{Bmatrix} M_{11} \\ M_{22} \\ M_{12} \end{Bmatrix} = \begin{bmatrix} B_{11} & B_{12} & B_{16} \\ B_{12} & B_{22} & B_{26} \\ B_{16} & B_{26} & B_{66} \end{bmatrix} \begin{Bmatrix} \epsilon_{11}^{(0)} \\ \epsilon_{22}^{(0)} \\ \epsilon_{12}^{(0)} \end{Bmatrix} + \begin{bmatrix} D_{11} & D_{12} & D_{16} \\ D_{12} & D_{22} & D_{26} \\ D_{16} & D_{26} & D_{66} \end{bmatrix} \begin{Bmatrix} \epsilon_{11}^{(1)} \\ \epsilon_{22}^{(1)} \\ \epsilon_{12}^{(1)} \end{Bmatrix} + \begin{bmatrix} F_{11} & F_{12} & F_{16} \\ F_{12} & F_{22} & F_{26} \\ F_{16} & F_{26} & F_{66} \end{bmatrix} \begin{Bmatrix} \epsilon_{11}^{(3)} \\ \epsilon_{22}^{(3)} \\ \epsilon_{12}^{(3)} \end{Bmatrix}$$

$$- \begin{bmatrix} r_1 \beta_{11}^A + r_2 \beta_{11}^B + r_3 \beta_{11}^D + r_4 \beta_{11}^E & r_5 \beta_{11}^A + r_6 \beta_{11}^B + r_7 \beta_{11}^D + r_8 \beta_{11}^E & r_9 \beta_{11}^A + r_{10} \beta_{11}^B + r_{11} \beta_{11}^D + r_{12} \beta_{11}^E \\ r_1 \beta_{22}^A + r_2 \beta_{22}^B + r_3 \beta_{22}^D + r_4 \beta_{22}^E & r_5 \beta_{22}^A + r_6 \beta_{22}^B + r_7 \beta_{22}^D + r_8 \beta_{22}^E & r_9 \beta_{22}^A + r_{10} \beta_{22}^B + r_{11} \beta_{22}^D + r_{12} \beta_{22}^E \\ r_1 \beta_{12}^A + r_2 \beta_{12}^B + r_3 \beta_{12}^D + r_4 \beta_{12}^E & r_5 \beta_{12}^A + r_6 \beta_{12}^B + r_7 \beta_{12}^D + r_8 \beta_{12}^E & r_9 \beta_{12}^A + r_{10} \beta_{12}^B + r_{11} \beta_{12}^D + r_{12} \beta_{12}^E \end{bmatrix} \begin{Bmatrix} T_0 \\ T_1 \end{Bmatrix}$$

($r_2 = r_7 = 1$)

(higher order bending constitutive relation)

$$\begin{Bmatrix} P_{11} \\ P_{22} \\ P_{12} \end{Bmatrix} = \begin{bmatrix} E_{11} & E_{12} & E_{16} \\ E_{12} & E_{22} & E_{26} \\ E_{16} & E_{26} & E_{66} \end{bmatrix} \begin{Bmatrix} \epsilon_{11}^{(0)} \\ \epsilon_{22}^{(0)} \\ \epsilon_{12}^{(0)} \end{Bmatrix} + \begin{bmatrix} F_{11} & F_{12} & F_{16} \\ F_{12} & F_{22} & F_{26} \\ F_{16} & F_{26} & F_{66} \end{bmatrix} \begin{Bmatrix} \epsilon_{11}^{(1)} \\ \epsilon_{22}^{(1)} \\ \epsilon_{12}^{(1)} \end{Bmatrix} + \begin{bmatrix} H_{11} & H_{12} & H_{16} \\ H_{12} & H_{22} & H_{26} \\ H_{16} & H_{26} & H_{66} \end{bmatrix} \begin{Bmatrix} \epsilon_{11}^{(3)} \\ \epsilon_{22}^{(3)} \\ \epsilon_{12}^{(3)} \end{Bmatrix}$$

$$- \begin{bmatrix} r_1 \beta_{11}^E + r_2 \beta_{11}^F + r_3 \beta_{11}^G + r_4 \beta_{11}^H & r_5 \beta_{11}^E + r_6 \beta_{11}^F + r_7 \beta_{11}^G + r_8 \beta_{11}^H & r_9 \beta_{11}^E + r_{10} \beta_{11}^F + r_{11} \beta_{11}^G + r_{12} \beta_{11}^H \\ r_1 \beta_{22}^E + r_2 \beta_{22}^F + r_3 \beta_{22}^G + r_4 \beta_{22}^H & r_5 \beta_{22}^E + r_6 \beta_{22}^F + r_7 \beta_{22}^G + r_8 \beta_{22}^H & r_9 \beta_{22}^E + r_{10} \beta_{22}^F + r_{11} \beta_{22}^G + r_{12} \beta_{22}^H \\ r_1 \beta_{12}^E + r_2 \beta_{12}^F + r_3 \beta_{12}^G + r_4 \beta_{12}^H & r_5 \beta_{12}^E + r_6 \beta_{12}^F + r_7 \beta_{12}^G + r_8 \beta_{12}^H & r_9 \beta_{12}^E + r_{10} \beta_{12}^F + r_{11} \beta_{12}^G + r_{12} \beta_{12}^H \end{bmatrix} \begin{Bmatrix} T_0 \\ T_1 \end{Bmatrix}$$

(linear and higher order transverse shearing constitutive relation)

$$\begin{Bmatrix} Q_2 \\ Q_1 \end{Bmatrix} = \begin{bmatrix} A_{44} & A_{45} \\ A_{45} & A_{55} \end{bmatrix} \begin{Bmatrix} \gamma_2^{(0)} \\ \gamma_1^{(0)} \end{Bmatrix} + \begin{bmatrix} D_{44} & D_{45} \\ D_{45} & D_{55} \end{bmatrix} \begin{Bmatrix} \gamma_2^{(2)} \\ \gamma_1^{(2)} \end{Bmatrix}, \quad \begin{Bmatrix} S_2 \\ S_1 \end{Bmatrix} = \begin{bmatrix} D_{44} & D_{45} \\ D_{45} & D_{55} \end{bmatrix} \begin{Bmatrix} \gamma_2^{(0)} \\ \gamma_1^{(0)} \end{Bmatrix} + \begin{bmatrix} F_{44} & F_{45} \\ F_{45} & F_{55} \end{bmatrix} \begin{Bmatrix} \gamma_2^{(2)} \\ \gamma_1^{(2)} \end{Bmatrix}$$

heat flow ↔ thermal gradient

(2D Fourier law)

$$\begin{Bmatrix} q_1^{(0)} \\ q_2^{(0)} \end{Bmatrix} = \begin{bmatrix} r_1 \lambda_{11}^A + r_2 \lambda_{11}^B + r_3 \lambda_{11}^D + r_4 \lambda_{11}^E & r_1 \lambda_{12}^A + r_2 \lambda_{12}^B + r_3 \lambda_{12}^D + r_4 \lambda_{12}^E \\ r_1 \lambda_{12}^A + r_2 \lambda_{12}^B + r_3 \lambda_{12}^D + r_4 \lambda_{12}^E & r_5 \lambda_{22}^A + r_6 \lambda_{22}^B + r_7 \lambda_{22}^D + r_8 \lambda_{22}^E \end{bmatrix} \begin{Bmatrix} g_1^{(0)} \\ g_2^{(0)} \end{Bmatrix}$$

$$+ \begin{bmatrix} r_5 \lambda_{11}^A + r_6 \lambda_{11}^B + r_7 \lambda_{11}^D + r_8 \lambda_{11}^E & r_9 \lambda_{11}^A + r_{10} \lambda_{11}^B + r_{11} \lambda_{11}^D + r_{12} \lambda_{11}^E \\ r_5 \lambda_{12}^A + r_6 \lambda_{12}^B + r_7 \lambda_{12}^D + r_8 \lambda_{12}^E & r_9 \lambda_{12}^A + r_{10} \lambda_{12}^B + r_{11} \lambda_{12}^D + r_{12} \lambda_{12}^E \end{bmatrix} \begin{Bmatrix} g_1^{(1)} \\ g_2^{(1)} \end{Bmatrix} + \begin{Bmatrix} r_9 \lambda_{11}^A + r_{10} \lambda_{11}^B + r_{11} \lambda_{11}^D + r_{12} \lambda_{11}^E \\ r_9 \lambda_{12}^A + r_{10} \lambda_{12}^B + r_{11} \lambda_{12}^D + r_{12} \lambda_{12}^E \end{Bmatrix}$$

$$\begin{Bmatrix} q_1^{(1)} \\ q_2^{(1)} \end{Bmatrix} = \begin{bmatrix} r_1 \lambda_{11}^B + r_2 \lambda_{11}^D + r_3 \lambda_{11}^E + r_4 \lambda_{11}^F & r_1 \lambda_{12}^B + r_2 \lambda_{12}^D + r_3 \lambda_{12}^E + r_4 \lambda_{12}^F \\ r_1 \lambda_{12}^B + r_2 \lambda_{12}^D + r_3 \lambda_{12}^E + r_4 \lambda_{12}^F & r_5 \lambda_{22}^B + r_6 \lambda_{22}^D + r_7 \lambda_{22}^E + r_8 \lambda_{22}^F \end{bmatrix} \begin{Bmatrix} g_1^{(0)} \\ g_2^{(0)} \end{Bmatrix}$$

$$+ \begin{bmatrix} r_5 \lambda_{11}^B + r_6 \lambda_{11}^D + r_7 \lambda_{11}^E + r_8 \lambda_{11}^F & r_9 \lambda_{11}^B + r_{10} \lambda_{11}^D + r_{11} \lambda_{11}^E + r_{12} \lambda_{11}^F \\ r_5 \lambda_{12}^B + r_6 \lambda_{12}^D + r_7 \lambda_{12}^E + r_8 \lambda_{12}^F & r_9 \lambda_{12}^B + r_{10} \lambda_{12}^D + r_{11} \lambda_{12}^E + r_{12} \lambda_{12}^F \end{bmatrix} \begin{Bmatrix} g_1^{(1)} \\ g_2^{(1)} \end{Bmatrix} + \begin{Bmatrix} r_{10} \lambda_{11}^B + r_{11} \lambda_{11}^D + r_{12} \lambda_{11}^E \\ r_{10} \lambda_{12}^B + r_{11} \lambda_{12}^D + r_{12} \lambda_{12}^E \end{Bmatrix}$$

($r_1 = r_2 = r_3 = r_6 = 1$)

internal energy ↔ temperature

$$\begin{Bmatrix} b^{(0)} \\ b^{(1)} \end{Bmatrix} = \begin{bmatrix} r_1 C^A + r_2 C^B + r_3 C^D + r_4 C^E \\ r_1 C^B + r_2 C^D + r_3 C^E + r_4 C^F \end{bmatrix} \begin{Bmatrix} T_0 \\ T_1 \end{Bmatrix} + \begin{bmatrix} r_5 C^A + r_6 C^B + r_7 C^D + r_8 C^E \\ r_5 C^B + r_6 C^D + r_7 C^E + r_8 C^F \end{bmatrix} \begin{Bmatrix} T_0 \\ T_1 \end{Bmatrix}$$

($r_1 = r_6 = 1$)

interaction energy ↔ strain

$$\begin{Bmatrix} a^{(0)} \\ a^{(1)} \end{Bmatrix} = T_{ref} \begin{bmatrix} \beta_{11}^A & \beta_{22}^A & \beta_{12}^A & \beta_{11}^B & \beta_{22}^B & \beta_{12}^B & \beta_{11}^D & \beta_{22}^D & \beta_{12}^D & \beta_{11}^E & \beta_{22}^E & \beta_{12}^E \\ \beta_{11}^B & \beta_{22}^B & \beta_{12}^B & \beta_{11}^D & \beta_{22}^D & \beta_{12}^D & \beta_{11}^E & \beta_{22}^E & \beta_{12}^E & \beta_{11}^F & \beta_{22}^F & \beta_{12}^F \end{bmatrix} \begin{Bmatrix} \epsilon_{11}^{(0)} & \epsilon_{22}^{(0)} & \epsilon_{12}^{(0)} & \epsilon_{11}^{(1)} & \epsilon_{22}^{(1)} & \epsilon_{12}^{(1)} & \epsilon_{11}^{(3)} & \epsilon_{22}^{(3)} & \epsilon_{12}^{(3)} \end{Bmatrix}^T$$

inertial quantities

$$(I_0, I_1, I_2, I_3, I_4, I_6) = \sum_{k=1}^N \int_{z_k}^{z_{k+1}} \rho^{(k)}(1, z, z^2, z^3, z^4, z^6) dz$$

elastic stiffnesses

$$(A_{ij}, B_{ij}, D_{ij}, E_{ij}, F_{ij}, H_{ij}) = \sum_{k=1}^N \int_{z_k}^{z_{k+1}} \bar{Q}_{ij}^{(k)}(1, z, z^2, z^3, z^4, z^6) dz$$

thermoelastic stiffnesses

$$(\beta_{ij}^A, \beta_{ij}^B, \beta_{ij}^D, \beta_{ij}^E, \beta_{ij}^F, \beta_{ij}^G, \beta_{ij}^H) = \sum_{k=1}^N \int_{z_k}^{z_{k+1}} \beta_{ij}^{(k)}(1, z, z^2, z^3, z^4, z^5, z^6) dz$$

thermal conductivities

$$(\lambda_{ij}^A, \lambda_{ij}^B, \lambda_{ij}^D, \lambda_{ij}^E, \lambda_{ij}^F, \lambda_{ij}^H) = \sum_{k=1}^N \int_{z_k}^{z_{k+1}} \lambda_{ij}^{(k)}(1, z, z^2, z^3, z^4, z^6) dz$$

thermal capacities

$$(C^A, C^B, C^D, C^E, C^F) = \sum_{k=1}^N \int_{z_k}^{z_{k+1}} C^{(k)}(1, z, z^2, z^3, z^4) dz$$

Fig. 4. Particularization of phenomenology equations of the unified scheme of Fig.1 for TTC and CTC (yellow-marked parts skipped or given values) models, along with the lamina-based orthotropic laminate quantities (bottom block).

If the above conditions are satisfied, and single-mode approximations with proper shape functions are taken for the sole mechanical (w , ϕ_1 , ϕ_2) and thermal (T_0 , T_1) 2D variables in Eqs. 13(b,c,d), it is possible to solve the in-plane fundamental mechanical equations of the continuous model (looking at them as a linear differential system) in terms of the corresponding variables u and v , thus slaving them to the reduced components of the other configuration variables in the following implicit form

$$u = f_u(W, \Phi_1, \Phi_2, T_{R0}, T_{R1}), \quad v = f_v(W, \Phi_1, \Phi_2, T_{R0}, T_{R1}) \quad (15)$$

where Φ_1 e Φ_2 appear only for the TTC model. Equations (15) take the role of the relevant independent approximations (Eqs. 13(a,b)) and also satisfy identically the boundary conditions on the plate edges where u and v appear. Thus, the reduced components U and V (directly associated with u and v) are no more present, and a first dimensional reduction of the mechanical problem can be achieved by applying the Galerkin method to the remaining fundamental equations of the continuous model, i.e. the three (one) out-of-plane mechanical and the two thermal equations of the TTC (CTC) model. Indeed, by neglecting rotational inertia in the transverse equation, where a linear viscous term is also inserted (for both TTC and CTC), and disregarding inertia and external moments $F_1^{(1)}$ and $F_2^{(1)}$ (for TTC) in the shear rotation equations, five (three) reduced ODEs can be obtained for the TTC (CTC) model, with three (one) mechanical and two thermal unknown reduced components. Analytical details are given in [42,44].

For the TTC model, a second kinematic condensation can be suitably performed at the 0D level on the two reduced shear rotation equations (thought as a linear algebraic system), if disregarding mechanical coupling terms of the type $\Phi_1 W^2$ and $\Phi_2 W^2$ occurring in them. This allows to slave the shear rotation components Φ_1 and Φ_2 to the remaining reduced components in the following implicit form

$$\Phi_1 = f_{\Phi_1}(W, T_{R0}, T_{R1}), \quad \Phi_2 = f_{\Phi_2}(W, T_{R0}, T_{R1}) \quad (16)$$

which take the role of the relevant independent approximations (Eqs. 13(d,e)) and also satisfy identically the boundary conditions on the plate edges where ϕ_1 and ϕ_2 appear. Thus, also the reduced components Φ_1 and Φ_2 (directly associated with ϕ_1 and ϕ_2) are no more present, and a further dimensional reduction of the thermomechanical problem is possible. Indeed, Equations (16) are inserted into the transversal equation of the reduced model, ending up to a system of three ODEs, one mechanical and two thermal, in the corresponding unknown reduced components, as for the CTC model. Analytical details can be found in [44,53], where this has been accomplished by considering the following set of single mode approximations for the 2D transverse displacement, the shear rotations, and the membrane/bending temperatures:

$$w(x, y, t) = W(t) \sin \frac{\pi x}{a} \sin \frac{\pi y}{b} \quad (17a)$$

$$\phi_1(x, y, t) = \Phi_1(t) \cos \frac{\pi x}{a} \sin \frac{\pi y}{b} \quad (17b)$$

$$\phi_2(x, y, t) = \Phi_2(t) \sin \frac{\pi x}{a} \cos \frac{\pi y}{b} \quad (17c)$$

$$T_0(x, y, t) = T_{R0}(t) \sin \frac{\pi x}{a} \sin \frac{\pi y}{b} \quad (17d)$$

$$T_1(x, y, t) = T_{R1}(t) \sin \frac{\pi x}{a} \sin \frac{\pi y}{b} \quad (17e)$$

In Eqs. (17a-e), mechanical eigenfunctions of the rectangular plate and dome shape distributions of the two unknown thermal variables have been assumed for the shape functions in Eqs. (13b-d), the former and latter satisfying simply supported and null (i.e. isothermal) boundary conditions along the plate edges, respectively.

Overall, the plate thermomechanical problem is reduced to three reduced ODEs in terms of time-dependent amplitudes W , T_{R0}, T_{R1} for both TTC and CTC models. It is worth noting that a similar reduction can be accomplished also for the (richer) modified models in Fig. 2, besides for the classical FTC one, but not for the general models therein indicated.

Different mechanical and thermal boundary conditions can be imposed at the plate edges, and thermal conditions in Eqs. (4-7) (or combinations of them) can be assumed on the external surfaces for the TTC model, whereas the CTC model can only account for free heat exchange due to the related linear temperature assumption along the thickness. If the prescribed thermal quantities on the external surfaces are constant, the previous reduction procedure can be performed without making the coefficients r_i of Eq. (10) explicit, thus obtaining the general system

$$a_{11}\dot{W} + a_{12}\dot{W} + (a_{13} + a_{14}p + a_{15}r_9 + a_{16}r_{11} + (a_{17}r_1 + a_{18}r_3)T_{R0} + (a_{19}r_5 + a_{110}r_7)T_{R1})W + a_{111}W^3 + (a_{112}r_2 + a_{113}r_4)T_{R0} + (a_{114}r_6 + a_{115}r_8)T_{R1} + a_{116}F_3^{(0)} = 0 \quad (18a)$$

$$a_{21}r_{11} + (a_{22}r_1 + a_{23}r_3)\dot{T}_{R0} + (a_{24}r_1 + a_{25}r_3)T_{R0} + a_{26}r_7T_{R1} + (a_{27}r_5 + a_{28}r_7)\dot{T}_{R1} + a_{29}\dot{W} \cdot W + a_{210}E^{(0)} = 0 \quad (18b)$$

$$a_{31}r_{12} + (a_{32}r_6 + a_{33}r_8)\dot{T}_{R1} + (a_{34}r_6 + a_{35}r_8)T_{R1} + a_{36}r_4T_{R0} + (a_{37}r_2 + a_{38}r_4)\dot{T}_{R0} + a_{39}\dot{W} + a_{310}E^{(1)} = 0 \quad (18c)$$

that for TTC includes all possible boundary conditions (or combinations of them) in Eqs. (4-7). Coefficients a_{ij} in Eqs. (18) have constant expressions that incorporate the features and physical properties of the considered model. The explicit version of the minimal system of ODEs for a specific set of upper/lower thermal conditions is obtained by substituting the expressions of the corresponding coefficients r_i .

If, on the other hand, the prescribed thermal quantities on the external surfaces are space/time dependent, the variation of the r_i coefficients from one thermal condition to the other has to be taken into account before discretizing the continuous model. Explicit expressions of the three ODEs provided for the TTC model by the reduction procedure when considering different combinations of in-plane mechanical and upper/lower thermal boundary conditions, with the latter entailing different coupling terms, are given in [41,44,45].

Of course, from a nonlinear dynamics viewpoint, it is important to note that reducing the transverse mechanical problem to a single ODE, as in Eqs. (18(a)), makes sense only if assuming to excite transversally (and possibly resonantly) the sole plate mode considered in Eq. 17(a), in the absence of whatever internal resonance with other transversal modes.

To give an example of explicit reduced ODEs, let us consider (i) simply supported, movable, and isothermal edges, subject to uniform stretching forces of magnitudes $p_x = p_y = p$ in x and y direction, and (ii) free heat exchange on the upper and lower surfaces, which is the sole case to be possibly addressed with the simpler CTC model. The explicit ODEs of the CTC-based minimal ROM are reported in Fig. 5, similar to the unified 2D scheme in Fig. 1(b) which highlights the fundamental governing PDEs. The reduced ODEs are embedded within the underlying unified 0D scheme, with configuration, phenomenological and balance equations/quantities schematically indicated, by also referring to an associated mechanical type body diagram of the minimal ROM, with the meaning of the involved symbols reported in the figure caption. It schematizes in mechanical terms also the thermal aspects of the problem, and interprets the effects of the multiphysics coupling as problem-dependent configuration distortions applied to each component oscillator. The coefficients a_{ij} in the three ODEs of Fig. 5 are renumbered in a sequentially suitable way with respect to those in Eqs. 18. Note that the structure of the three equations also holds for the TTC model (of course if considering the same mechanical and thermal boundary conditions), but the expressions of the coefficients a_{ij} are different, the TTC ones being more involved and incorporating the underlying higher order displacement and temperature assumptions.

For the TTC model, the reduced modeling framework in Fig. 5 can be suitably used to compare a variety of minimal ROMs ensuing from different prescriptions of thermal boundary conditions on the plate external surfaces. A number of them will be presented forward, when validating the general reduction procedure in mechanical and thermal terms (Sect. 4) and investigating the relevant nonlinear dynamics (Sect. 5). The unified framework is also useful for controllably deriving and comparing TTC- or CTC-based ROMs of even lower dimension, possibly ensuing from different approximations about the comparative significance of membrane and bending thermal dynamics and/or the actual importance of mechanical coupling terms in thermal equations. Indeed, the former may allow a further reduction to two reduced ODEs, still working in a two-way thermomechanical coupling perspective, while the latter, which also entail a possible one-way coupling formulation of the thermomechanical problem, may end up to even a single uncoupled (mechanical) ODE with prescribed thermal distortions. The matter will be addressed in Sect. 6.

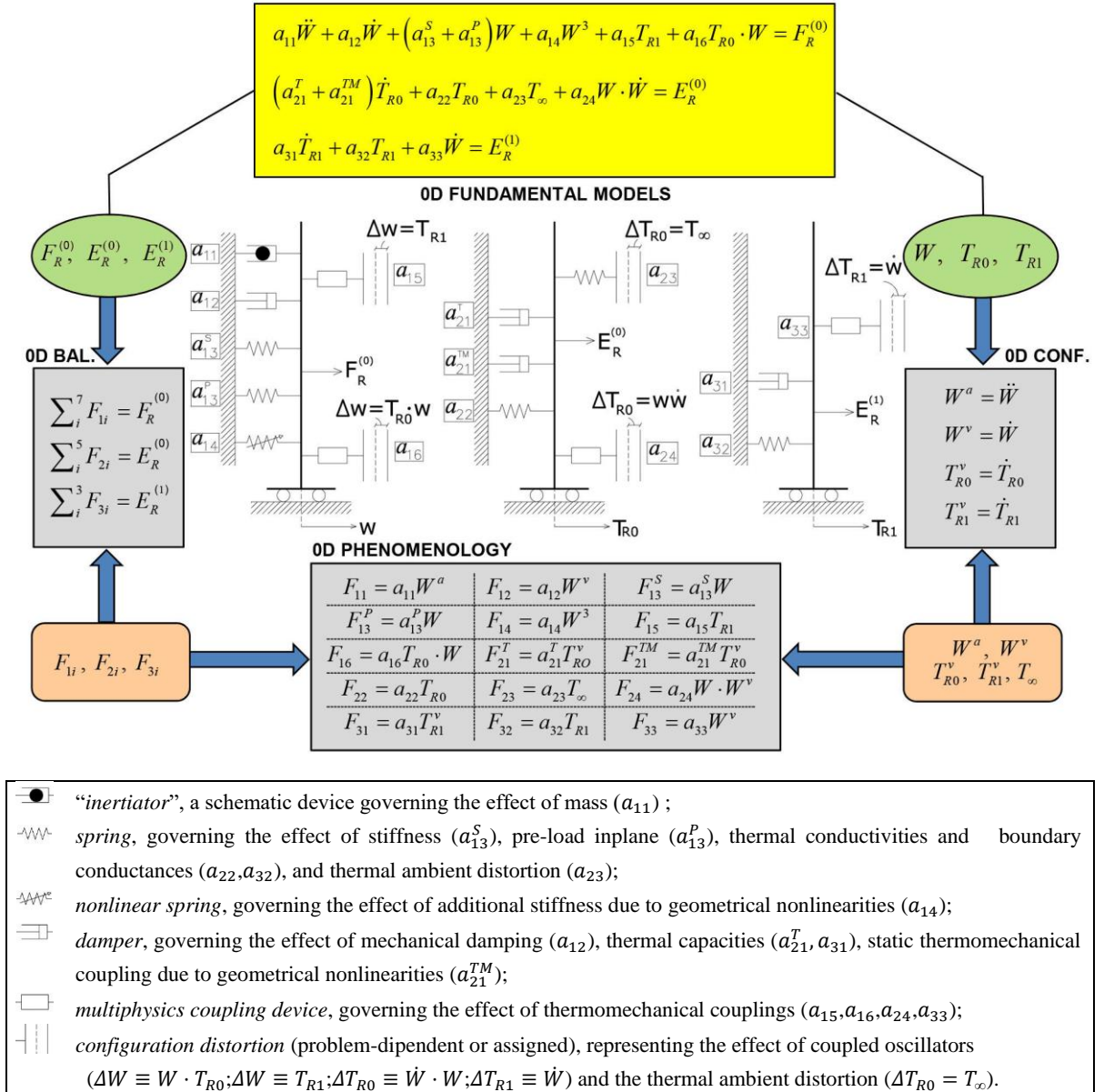


Fig. 5. Particularization of the unified scheme of Fig. 1 for 0D CTC-based minimal ROM: ODEs for two-way thermomechanical coupling (yellow block), with a corresponding mechanical-type body diagram and meaning of the involved symbols.

4. Validation of minimal ROMs

This section presents a validation of the previously discussed minimal models, aimed at reliably using them for a following systematic investigation of the nonlinear dynamics of a class of thermomechanically coupled plates. Validation is performed by comparing outcomes provided by the reduced models as regards some aspects of mechanical and thermal response with correspondingly available literature results and/or with outcomes provided by richer models, i.e. higher-order ROMs and/or finite elements.

4.1 Linear dynamics and buckling

Linear models extracted from minimal nonlinear ROMs allow to obtain numerical benchmarks as regards linear dynamics. A first comparison with literature results is concerned with natural frequencies [44]. Table 2 reports frequency values provided by TTC and CTC models for a square isotropic plate with different thickness ratios a/h , by either considering thermomechanical formulations or removing the corresponding thermal parts (M label in the table). Results are compared with those provided by the Carrera Unified Formulation (CUF) handling in a unified manner a large variety of plate theories [13,55], by considering a layer-wise plate with fourth-order expansion of displacements and temperature along the thickness (LD4) or a shear-undeformable plate (CLT), with (TM label) or without thermal effects. The agreement between TTC and LD4 values (the latter representing the most refined CUF model) is remarkable also for stubby plates, where the more constrained shear-undeformable models provide notably higher frequency values. Overall, the effect of thermomechanical coupling is very small and can be discarded in free vibration analysis. Anyway, it usually provides slightly higher frequencies than pure mechanical models because it acts like a thermal source which leads to a larger global stiffness of the plate. TTC* model of the reduced formulation assumes that the temperature on the external surfaces equals the external room temperature and allows to reproduce the fourth-order layer-wise profile obtained with LD4(TM)* [13] in the same external thermal conditions, as shown in Fig. 6. Compared to LD4-models (fourth-order expansion of configuration variables), TTC-models (third-order expansion of configuration variables) show values slightly higher, due to their greater internal constraint.

A second comparison with literature results is concerned with mechanical and thermal buckling. Table 3 reports critical buckling loads provided by several models for two thickness ratios of the square isotropic plate. As to thermal buckling, either a dome-shaped or a uniform distribution of temperature over the plate upper surface is considered (Fig. 7), the former being a good idealization better reproducing experimental data about the actual temperature distribution over a hot structural panel even under uniform surface heat flux, due to the existence of supporting cooler boundary heat sinks [56]. Buckling values obtained by the CTC model are identical to the mechanical and thermal ones provided by the Navier solution [49] and minimum potential energy [56], respectively, for the Kirchhoff plate. TTC values are as much lower than CTC ones as the plate becomes thicker, due to the higher deformability of the former. Analytical details for both models are available in [44].

Table 2. Fundamental frequency (Hz) for the isotropic plate, with several models and thickness ratios a/h . (M) ((TM)) means thermal part of the model removed (included). LD4 refers to layer-wise plate with fourth-order expansion of displacements and temperature along the thickness, CLT refers to Kirchhoff plate. (*) means that the temperature on the external surfaces equals the external room temperature.

		a/h	2	5	10	50	100
ROMs	TTC		779.56	175.87	47.436	1.9492	0.4877
	TTC*		779.42	175.16	47.211	1.9492	0.4877
	TTC(M)		777.95	175.16	47.211	1.9394	0.4852
	CTC		1219.68	195.15	48.787	1.9515	0.4878
	CTC(M)		1213.56	194.16	48.542	1.9416	0.4854
CUF	LD4(TM) [13]		763.03	173.10	47.158	1.9481	0.4875
	LD4(TM)* [13]		765.32	172.88	47.094	1.9454	0.4869
	LD4 [13]		763.94	172.40	46.946	1.9390	0.4852
	CLT(TM) [13]		1031.3	189.87	48.607	1.9596	0.4900
	CLT [13]		1021.5	188.08	48.148	1.9411	0.4854

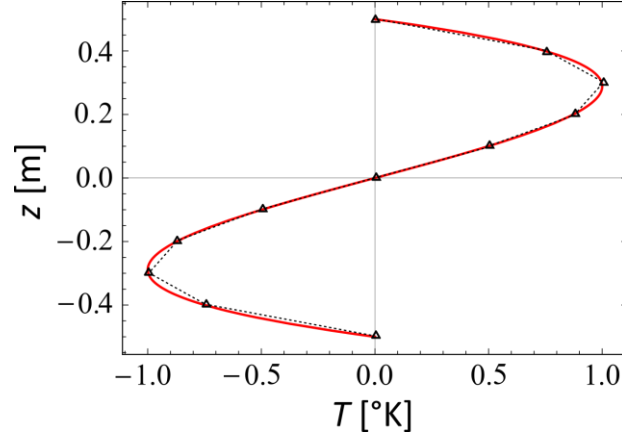


Fig. 6. Temperature profile along the plate thickness: comparison between layer-wise plate with fourth-order expansion of temperature along the thickness (LD4(TM)*, black triangles) and the present model based on single-layer approach with third-order expansion of the temperature along the thickness (TTC*, red line).

4.2 3D spatiotemporal thermal dynamics

A major novelty of the accomplished continuum formulation and the ensuing minimal modelling stands in complementing the assumed out-of-plane distribution of the mechanical variable with a consistent description of the transverse temperature which, depending on the assumptions refinement, allows (or not) to deal with the variety of thermal excitations of possible interest in technical applications, mostly as regards prescribable boundary conditions. Thus, one more validation step consists of focusing on the sole thermal aspects, and comparing the relevant responses provided by TTC and CTC models, in both transient and steady regimes, to those obtained by reduced thermal models of higher-order, by analytical solutions, and/or by finite elements. This also allows to get a comprehensive and reliable understanding of the spatio-temporal thermal dynamics entailed by different excitations.

Within the criterion of an assumed, unknown, temperature distribution along the thickness, at the base of thermomechanical formulation, a suitable richer thermal model is characterized by a polynomial seventh order shape of the 3D temperature:

$$T(x, y, z, t) = T_0 + zT_1 + z^2T_2 + z^3T_3 + z^4T_4 + z^5T_5 + z^6T_6 + z^7T_7 \quad (19)$$

with 2D unknown components $T_i(x, y, t)$, $i = 0-7$, instead of the third- or first-order shapes (Eqs. (3) and (11)).

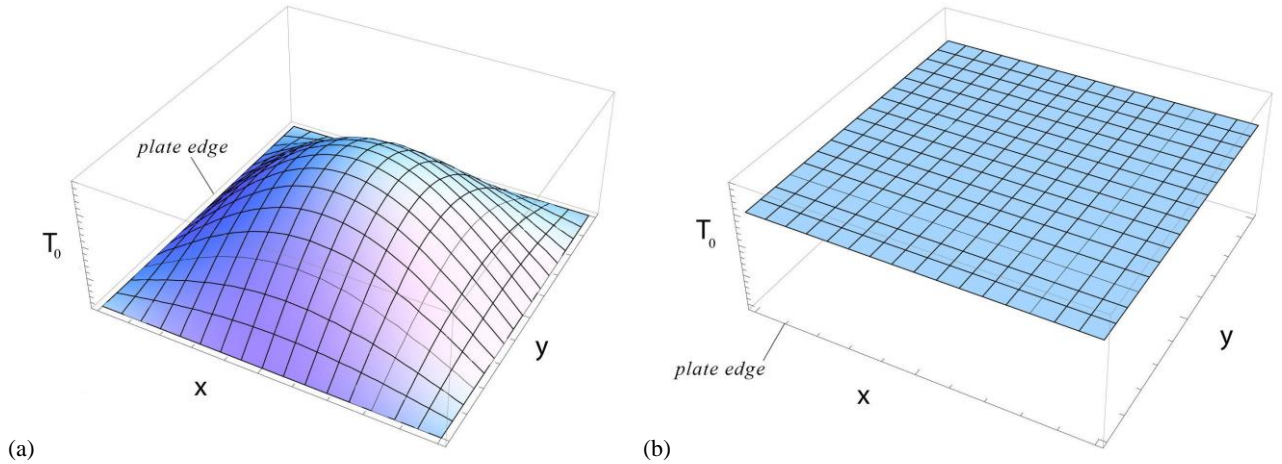


Fig 7. (a) Dome-shaped temperature distribution, (b) uniform temperature distribution.

Table 3. Critical buckling mechanical and thermal loads for the isotropic square plate, with several models and thickness ratios.

		a/h	20	100
Current	TTC mechanical buckling		16265 kN	131882 N
	CTC mechanical buckling		16494 kN	131956 N
	TTC thermal buckling, <i>dome-shaped</i> profile heating		346.352 K	14.041 K
	TTC thermal buckling, <i>uniform</i> profile heating,		124.774 K	5.058 K
	CTC thermal buckling, <i>dome-shaped</i> profile heating		351.235 K	14.049 K
	CTC thermal buckling, <i>uniform</i> profile heating,		126.533 K	5.061 K
Literature	mechanical buckling, via Kirchhoff plate-Navier solution [49]		16494 kN	131956 N
	thermal buckling, <i>dome-shaped</i> profile heating, via Kirchhoff p.- minimum p.energy [56]		351.235 K	14.049 K
	thermal buckling, <i>uniform</i> profile heating, via Kirchhoff p.- minimum p.energy [56]		126.533 K	5.061 K

As for the TTC model, thermal boundary conditions on upper/lower surfaces (Eqs. (4-7)) can be used to express two (out of eight) 2D components in terms of the others, and then to expand each of the remaining six independent components in terms of one corresponding 0D component $T_{Ri}(t)$, as of Eqs. 17(d,e) for TTC, overall ending up to six thermal unknowns of the reduced problem. The ensuing STC (Seventh-order theory with Thermomechanical Coupling) ROM is the minimal one for the new thermal sub-problem, which is considerably more involved than the TTC one for involving six ODEs instead of two. However, the new, richer, minimal ROM is more flexible than the TTC one because of allowing to consider also nonlinear body source energy and boundary edge conditions.

In the sequel, 3D spatio-temporal thermal regimes, both transient and steady, are reconstructed from the results of 0D reduced models via a backward procedure, for the three cases of thermal (boundary/body) excitations listed in Fig. 8. No mechanical coupling terms are considered in the TTC thermal Eqs. 18(b,c) (and in corresponding ones of the other ROMs), since their indirect effects on thermal dynamics are negligible with respect to the direct ones produced by the applied thermal loads [46]. Details of all analyses and results can be found in [45]. For all cases, elastic and thermal properties of the considered materials are assumed to be temperature-independent.

Case 1 refers to a square isotropic plate with AL2024 material [44], thickness ratio $a/h = 20$, and a spatially constant temperature $T^* = 100$ K prescribed also on the edges. Transient 3D temperature curves in the center of plate midplane are shown in Fig. 9a superposing results obtained with TTC and STC models, along with

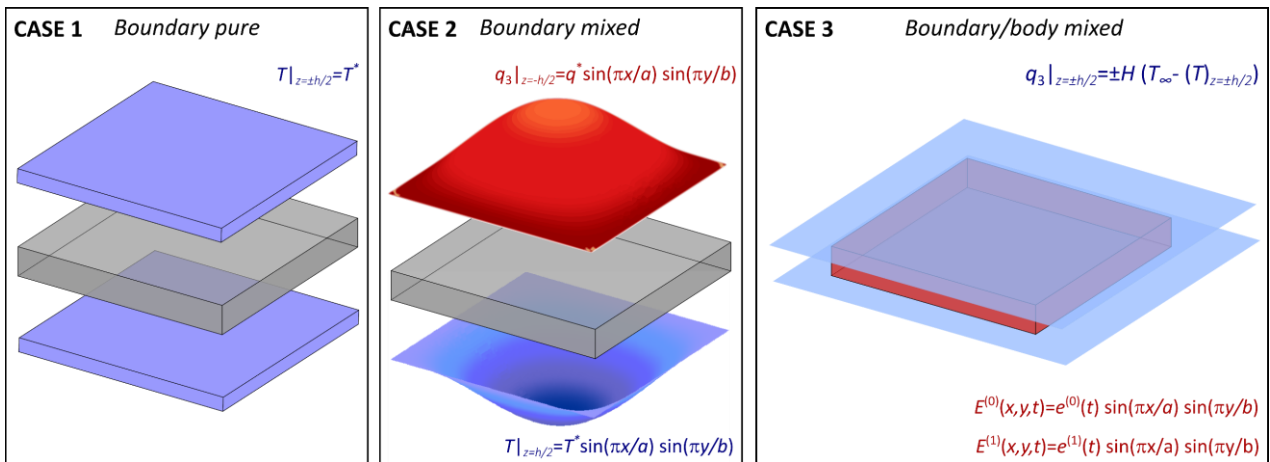


Fig 8. Three different cases of thermal (boundary/body) excitations: Case 1: constant temperature prescribed (up/down faces); Case 2: dome-shape irradiation flow (up face), dome-shape temperature prescribed (down face); Case 3: free heat exchange (up/down faces), active source (body)

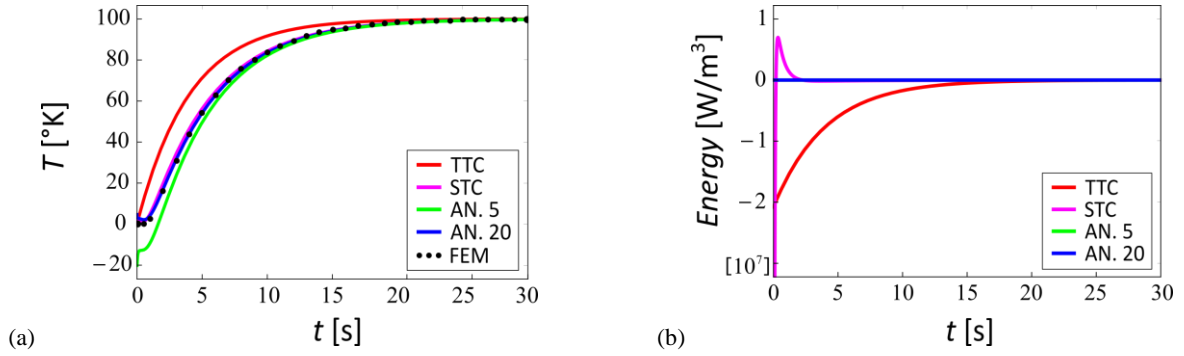


Fig 9. Case 1, constant temperature prescribed on up/down faces: time histories of (a) 3D temperature and (b) energy in the center of plate midplane. TTC (red), STC (magenta), analytical solutions with 5 (green) and 20 (blue) terms, finite element solution (black dots).

those provided by an analytical solution of non-stationary conduction with 5 or 20 terms in the series, assumed as benchmark [57], and by a finite element solution. The STC (blue) curve agrees very well with the nearly coinciding 20-term analytical (gray) and finite element (black dots) solutions, while the curve of the 5-term analytical solution (green) gives a bad estimate at the first seconds of conduction, because it starts from a high and unrealistic negative value, but then approaches the curves of greater precision. The TTC curve (red) correctly presents a zero value at the initial instant and grows without inflection points, however overestimating the transient temperature. Figure 6(b) reports the time history of total energy balance in the 3D membrane equation, showing a swift vanishing of the STC marked initial imbalance and a slower zeroing of the TTC one. But, overall, possible transient imbalance does not affect the steady response.

Still in the plate center, Figure 10 shows 3D temperature curves along the thickness at two, nearly initial (a) and intermediate (b), instants, along with the 3D internal energy curves for the latter (c). The STC temperature profile is very close to the 20-term analytical and finite element ones since the nearly initial instant, notwithstanding a slight internal energy difference still occurring at $t = 10$ s, while TTC exhibits a progressively vanishing (see Fig. 9(a)) temperature overestimation.

Figure 11 shows temperature graphs along x , at mid-plane level and y half-size. Remembering boundary conditions, at the nearly initial instant $t = 0.3$ s the real temperature is zero along the whole x direction except on the edges, where it is $T = 100$ K; therefore, in Fig. 11(a), STC (although providing the correct temperature in the centre) implies the same shape error of TTC, which persists at $t = 10$ s (Fig. 11c) and only vanishes in steady conditions. This is due to the different mathematical assumption for the prescribed constant temperature on the boundary with respect to the assumed internal 2D dome-shape temperatures (Eqs. 17(d,e)). To improve the approximation, multimodal instead of unimodal thermal shapes along x and y should be considered,

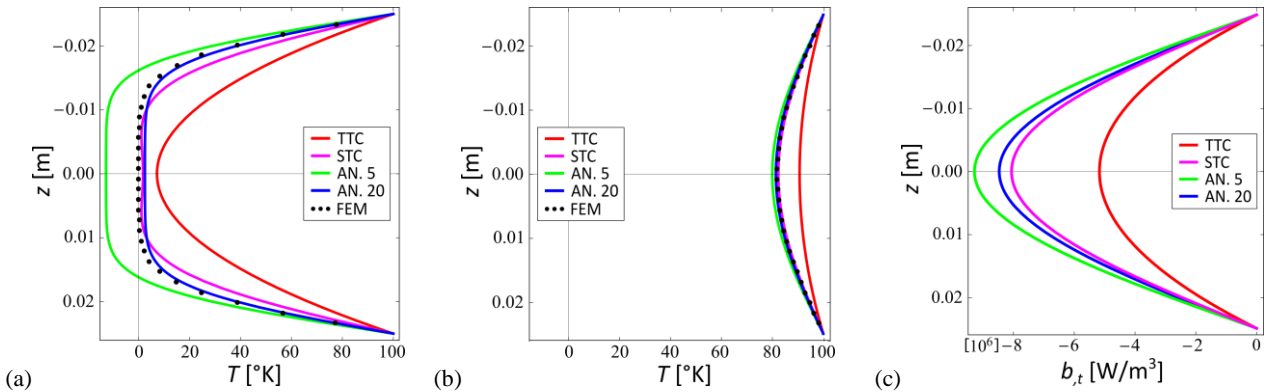


Fig 10. Case 1, constant temperature prescribed on up/down faces: Temperature profiles along the thickness in midpoint, at (a) $t = 0.3$ s, (b) $t = 10$ s, and (c) internal energy for the latter. TTC (red), STC (magenta), analytical solutions with 5 (green) and 20 (blue) terms, finite element solution (black dots).

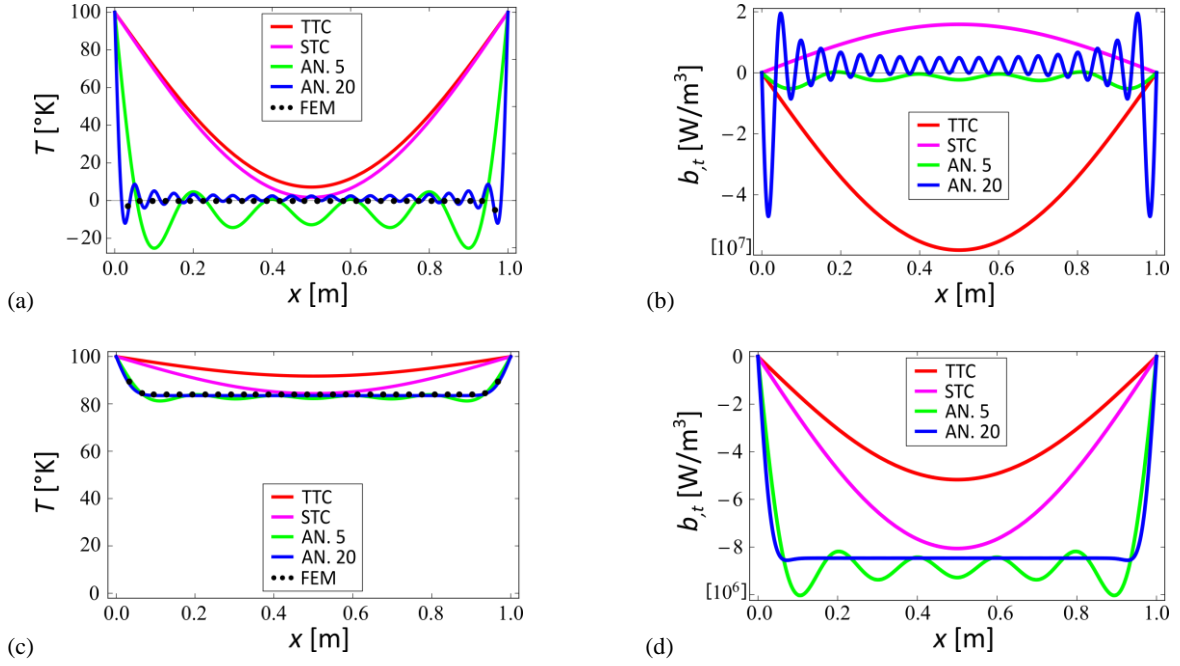


Fig 11. Case 1, constant temperature prescribed on up/down faces: Temperature (a,c) and internal energy (b,d) profiles along x at $y = b/2, z = 0$ and (a,b) $t = 0.3$ s, (c,d) $t = 10$ s. TTC (red), STC (magenta), analytical solutions with 5 (green) and 20 (blue) terms, finite element solution (black dots).

however nullifying the minimal ROM perspective. But the error shape will vanish if consistently considering for the temperature (or other thermal loads) prescribed on the external surfaces the same dome-shaped spatial distribution as the assumed 2D internal temperature one, as it will be done in the following excitation cases 2 and 3. Moreover, from the whole analysis of case 1, STC results are seen to be close to those of the 20-term analytical solution, also in the transient, and such to be reliably assumed as reference for further comparing cheaper ROMs such as TTC and CTC ones.

Case 2 refers to a square, single-layer, epoxy/carbon fibre composite [40], orthotropic and thicker ($a/h = 10$) plate with cold edges, subjected to a dome-shaped heat flow $q_3(x, y, z, t)$ on the upper surface and a dome-shaped temperature distribution (with $T^* = 10$ K) on the lower surface (Fig. 8). Since thermal loads are not symmetrical, also the reduced bending component $T_{R1}(t)$ is activated, contrary to Case 1, overall giving rise to the 3D temperature curves of STC (practically coinciding with finite element solution) and TTC in

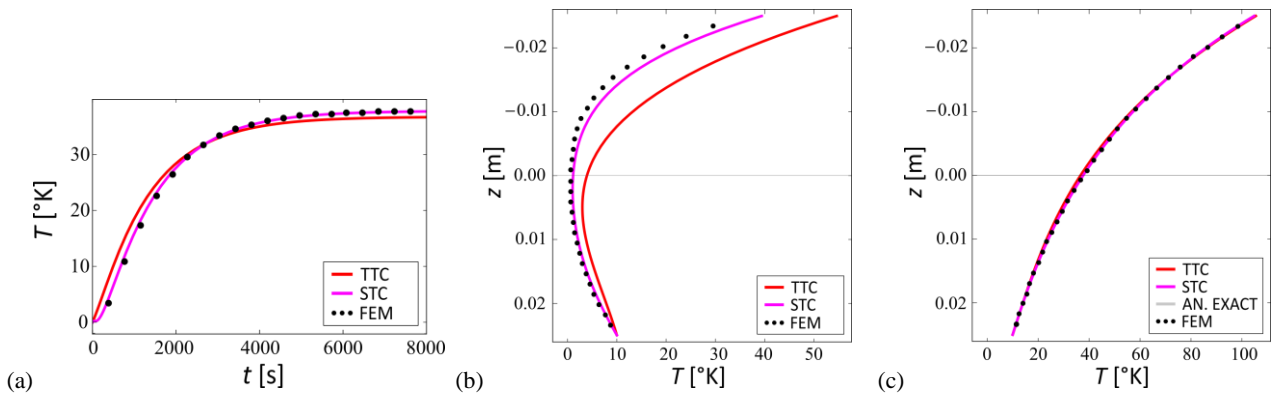


Fig 12. Case 2, dome-shaped flow and temperature prescribed on up/down faces: (a) time histories of temperature, (b,c) profiles along the thickness in midpoint, at $t = 200$ s and $t = 8000$ s. TTC (red), STC (magenta), exact stationary analytical solution (gray line in (c)), finite element solution (black dots).

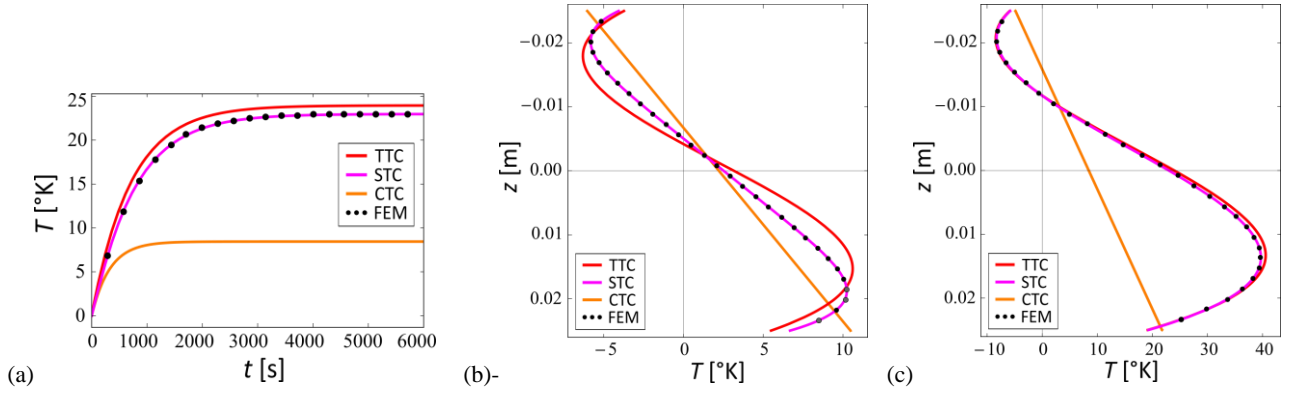


Fig 13. Case 3, free heat exchange on up/down faces and active body source: (a) time histories of temperature, (b,c) profiles along the thickness in midpoint, at $t = 100$ s and $t = 6000$ s. TTC (red), STC (magenta), CTC (orange), finite element solution (black dots).

Fig. 12(a), whose transients are much longer than those of Case 1 and very close to each other. Figure 12 also shows the corresponding temperature profiles along the thickness, in the central point of the plate. They are quite dissimilar at a nearly initial instant ($t = 200$ s) (b), mostly at the upper points far away from the midplane, but almost coincident at the stationary state ($t = 8000$ s) (c), where the STC profile perfectly coincides with finite elements and with the curve (gray, but not visible) of the exact stationary analytical solution [58].

Case 3 refers to the same plate with cold edges of case 2, subjected to a free convective exchange with the surrounding medium on the up/down faces, and to a body source energy inside the plate, with intensity linearly varying along the thickness between two assigned extreme values (Fig. 8). Since free heat exchange on external faces can be prescribed also in the CTC model, it is considered in the comparison, too. Figure 13a compares 3D temperature curves of TTC with those of STC and CTC, in the midpoint. CTC time history is far away from those of the other two models (with also a stationary value significantly lower), which instead are quite close to each other. Figure 13(b,c) shows the corresponding temperature profiles along the thickness, in the central point of the plate, at a nearly initial instant ($t = 100$ s) and at stationary state ($t = 6000$ s). All models exhibit a more marked temperature increase in the lower part of the plate, due to the considered power density distribution along the thickness (Fig. 8); however, the maxima of the more refined models are not located at the up/down surfaces, possibly due to heat dissipation towards the environment occurring therein. In the stationary phase (Fig. 13(c)), the CTC profile exhibits a considerable deviation from TTC and STC ones, which practically coincide with each other. Obviously, the CTC model is much penalized by the assumed linear temperature distribution (Eq. (11)), which entails analytical vanishing of the thermal flow contribution to the 3D balance, even though its overall effect along the thickness is taken into account in the 2D balance through the $Q^{(0)}$ and $Q^{(1)}$ contributions in Fig. 3(d) [42].

5. Nonlinear dynamics of TTC model

In view of a systematic, computationally heavy, yet reliable investigation of the nonlinear dynamics of two-way thermomechanically coupled plates with a corresponding ROM, it is important to identify an acceptably ‘best’ minimal model to use, as resulting from a compromise among different requirements. Features of

- functionality (ability to provide reliable descriptions of phenomena under examination),
 - richness (quantity and quality of nonlinear characteristics preserved from the underlying continuous formulation, in order to allow exhaustive descriptions of the involved dynamics),
 - flexibility (ability to consider a variety of thermomechanical assumptions, excitations and boundary conditions of technical interest),
 - cheapness (ability to reduce both computational and result interpretation burden),
- are considered.

From the thermal viewpoint, the analysis in Sect. 4.2 highlights the excellent capability of the minimal TTC model to account for a variety of excitations and boundary conditions of technical interest. It is much higher

than the CCT one (however with the same minimal structure of two ODEs/unknowns), while also providing a description of the spatiotemporal temperature field matching very well the ‘nearly exact’ steady one of STC (with minor differences in the transient), which however requires six ODEs/unknowns, thus being more involved in computational terms. In turn, CTC does not achieve such a good steady temperature description even for small plate thicknesses, mostly if considering greater intensities of thermal source energy [45].

From the mechanical and coupling viewpoints, TTC and CTC are practically ‘identical’ in the minimal reduction perspective (one and three ODEs/unknowns, respectively, and same structure), yet with the former model allowing to account also for third-order shear deformability (besides more thermal boundary conditions). The mechanical balance of STC might be reduced to a single equation, too, if neglecting displacement terms of order higher than cubic [45], possibly allowing for a more reliable description of thermal-to-mechanical coupling effects entailed by highly involved internal temperature fields. However, this would be somehow inconsistent with the assumed higher-order temperature distribution, and questionable if dealing with quite thick plates. Alternatively, a higher-order expansion should be assumed in Eqs. (17(a-c)) for the mechanical out-of-plane configuration variables, thus further increasing the overall number of reduced ODEs/unknowns.

All previous points highlight how TTC can represent the ‘best’ minimal model to use for systematic numerical investigations of the nonlinear dynamics of thermomechanically coupled symmetric cross-ply laminates. In the sequel, transient and steady responses under a variety of thermal (boundary and body) sources entailing direct activation of the temperature field, in addition to mechanical excitations, will be analysed, highlighting the influence of thermomechanical coupling and the non-trivial effects of slow thermal dynamics on the swift steady mechanical response via tools of local and global dynamics.

The set of dimensionless TTC (and CTC) two-way coupled governing ODEs (mechanical, thermal membrane, and thermal bending, sequentially), with a_{ij} now denoting nondimensional coefficients, is reported in Fig. 14, where mechanical and body thermal excitations are included, however without terms due to specific thermal boundary conditions. The distributed in-plane constant axial load p (see Fig. 2) enters the a_{13} coefficient of mechanical linear stiffness, transverse harmonic load (of amplitude f in the a_{17} coefficient) exciting the plate at primary resonance appears in the mechanical equation, and membrane (e_0) and bending (e_1) internal heat sources enter the corresponding thermal equations. Coupling terms in the three equations are framed by red boxes.

Specific thermal boundary conditions (b.c.) prescribed on the upper and lower surfaces add further terms as per the equations reported in Fig. 15, which refer to cases considered in the following investigations. The first set of equations (also holding for CTC) includes a new term (in red, with α_1 dimensional (in Kelvin⁻¹) coefficient of thermal expansion) in the membrane equation (the sole one directly activated, in the absence of e_0 and e_1), associated with a dimensional (in Kelvin) time-constant temperature difference T_∞ between plate and surrounding medium, which entails free heat exchange (FHE) on the up/down outer surfaces.

p : constant precompression f : amplitude of harmonic mechanical excitation

$$\dot{W}(t) + a_{12}\dot{W}(t) + a_{13}W(t) + a_{14}W(t)^3 + a_{15}T_{R1}(t) + a_{16}T_{R0}(t)W(t) + a_{17}Cos(t) = 0$$

$$\dot{T}_{R0}(t) + a_{22}T_{R0}(t) + a_{24}W(t)\dot{W}(t) + a_{25}e_0(t) = 0$$

$$\dot{T}_{R1}(t) + a_{32}T_{R1}(t) + a_{33}\dot{W}(t) + a_{34}e_1(t) = 0$$

e_1 : bending thermal excitation e_0 : membrane thermal excitation

Fig 14. General structure of two-way coupled ODEs (mechanical, thermal membrane, and thermal bending) for TTC (and CTC); red-squared terms account for the thermomechanical coupling, blue-squared terms represent mechanical and thermal excitations.

Free heat exchange (FHE): T_∞

$$\ddot{W}(t) + a_{12}\dot{W}(t) + a_{13}W(t) + a_{14}W(t)^3 + a_{15}T_{R1}(t) + a_{16}T_{R0}(t)W(t) + a_{17}\text{Cos}(t) = 0$$

$$T_{R0}^\cdot(t) + a_{22}T_{R0}(t) + \mathbf{a_{23}\alpha_1 T_\infty} + a_{24}W(t)\dot{W}(t) + a_{25}e_0(t) = 0$$

$$T_{R1}^\cdot(t) + a_{32}T_{R1}(t) + a_{33}\dot{W}(t) + a_{34}e_1(t) = 0$$

Prescribed constant (PPC) or dome-shaped (PPD) temperatures on the external surfaces: T_{up}, T_{down}

$$\ddot{W}(t) + a_{12}\dot{W}(t) + a_{13}W(t) + a_{14}W(t)^3 + a_{15}T_{R1}(t) + a_{16}T_{R0}(t)W(t) + a_{17}\text{Cos}(t) + \mathbf{a_{18}(T_{up}+T_{down})W} + \mathbf{a_{19}(T_{up}-T_{down})} = 0$$

$$T_{R0}^\cdot(t) + a_{22}T_{R0}(t) + \mathbf{a_{23}\alpha_1(T_{up}+T_{down})} + a_{24}W(t)\dot{W}(t) + a_{25}e_0(t) = 0$$

$$T_{R1}^\cdot(t) + a_{32}T_{R1}(t) + a_{33}\dot{W}(t) + a_{34}e_1(t) + \mathbf{a_{35}\alpha_1(T_{up}-T_{down})} = 0$$

Fig 15. General ODEs (Fig. 14) with additional terms due to different boundary conditions. Top block: Free heat exchange (FHE), one more (red) term in membrane equation. Bottom block: Prescribed prescribed constant (PPC) temperature, two more (red) terms in membrane and bending equations; prescribed prescribed dome-shape (PPD) temperature: two more (red) terms in membrane and bending equations, plus two more (blue) terms in mechanical equation.

The second set of ODEs holds for a prescribed spatial distribution of (possibly different) temperatures on the upper (T_{up}) and lower (T_{down}) surfaces, which (still in the absence of e_0 and e_1) entail direct activation of both membrane and bending thermal dynamics (indirect activation always occurs, due to the presence of mechanical coupling terms), unlike the FHE condition. Two different distributions are considered, constant (PPC: prescribed prescribed constant) or dome-shaped with T_{up}, T_{down} dimensional (in Kelvin) central values (PPD: prescribed prescribed dome-shape), both entailing additional (red) terms in the membrane and bending equations, with different a_{23}, a_{35} values. Coefficients of the other thermal terms are also different from the corresponding ones in FHE equations, because the physical processes activated by free heat exchange (convection plus conduction) and prescribed temperatures (only conduction) are different. The PPD b.c. also induce two (blue) additional terms in the mechanical equation, one affecting the linear mechanical stiffness (like the axial load), and the other adding a constant external excitation.

In the next sub-section, nonlinear dynamics of TTC model is investigated by considering a square orthotropic single-layer plate in epoxy/carbon fiber composite, with thickness ratio $a/h = 100$, subjected to mechanical loads consisting of in-plane pre-stressing axial force p in incipient buckling condition, and transverse harmonic excitation of amplitude f at primary resonance. As regards thermal loads, the capability of TTC model to account for different excitation conditions is highlighted by considering four different cases of either boundary conditions on external surfaces or body excitation, with also a comparative overview of the ensuing coupled thermomechanical responses. Material elastic and thermal properties are taken from [13], apart from a lower value of the specific heat considered in the first two cases for easier computation, and are assumed to be temperature-independent. Details of the various analyses can be found in [40,41,46].

First, FHE boundary condition (i.e., the first set of ODEs in Fig. 15) and bending body excitation e_1 are separately addressed, for being suitable reference cases to get an overall view of the effects of basic, yet qualitatively different, thermal excitations on the plate buckling/postbuckling, in both local and global dynamics terms. They also allow us to get a fundamental understanding of the important influence entailed by the slow thermal dynamics on the much swifter mechanical vibrations of the plate, as governed by the thermomechanical coupling. In both cases, the membrane body excitation e_0 is set to zero. Note that T_∞ and e_1 excitations can be dealt with also by the CTC model, which was indeed first used for systematic investigations of the relevant nonlinear responses [40]. When using TTC, local and global dynamics outcomes

of the thin plate considered here are essentially the same as CTC ones, which are thus referred to for summarizing the main features of dynamic buckling/post-buckling.

Then, the sole PPC or PPD boundary conditions (second set of ODEs in Fig. 15, with $e_0=e_1=0$) are considered, to highlight the great variety of buckled/post-buckled dynamical scenarios obtainable under different quantitative and qualitative prescriptions for the same kind of thermal excitation. Further on, thermal sources of different nature (boundary vs body) but possibly equivalent effects on the coupled thermomechanical response are also considered, dwelling on the similarity/difference of actual outcomes.

In all considered cases, the system response is described in terms of local and global dynamics. The first one is studied realizing bifurcation diagrams by means of the continuation software AUTO [59], which allows us to investigate existence and stability of periodic steady solutions as a function of selected parameters. The detected solutions are then characterized with phase portraits and temporal evolutions obtained by numerically integrating the ODEs with Wolfram Mathematica [60] software. The second one is addressed by constructing 2D cross sections of the 4D basins of attraction with a C++ ad hoc routine, which works by dividing the selected state plane in a grid of proper size and by locating the centers of the grid box from which the trajectories detected via quasi-Newton's method are followed. Overall, the fundamental role played by global dynamics analysis in unveiling meaningfully different outcomes of the mechanical response resulting from the slowness of thermal dynamics is addressed.

5.1 Dynamic buckling/post-buckling: a local and global analysis

Free heat exchange. The sole time-constant temperature difference T_∞ between plate and environment entails pure convection on external surfaces and pure internal conduction, with direct activation of the sole symmetric membrane thermal dynamics (T_{R0}), and the mechanical response altered thanks to the presence of the coupling linear term $a_{16}T_{R0}W$ which modifies the linear stiffness. In turn, a minor bending temperature T_{R1} is dragged by the mechanical coupling term $a_{33}\dot{W}(t)$. The bifurcation diagram of mechanical response with varying T_∞ is reported in Fig. 16(a) in terms of minimum and maximum response curves pointing out the evolution of corresponding overall amplitudes. If moving from a p -induced mechanical pre-buckling configuration in which the sole one-period response P1 exists, progressive warming of the environment (i.e., $T_\infty > 0$) entails onset of a first (P1^{III}/P1^{IV}) and then a second (P1^I/P1^{II}) couple of buckled solutions, oscillating around the varied positive/negative configurations of the plate. For $T_\infty = 190$ K, both couples are represented as high- (green/blue) and low- (orange/red) amplitude oscillations, respectively, in the phase portraits of Fig. 16(b), where the coexisting (gray) post-buckled cross-well response oscillating around both varied equilibria

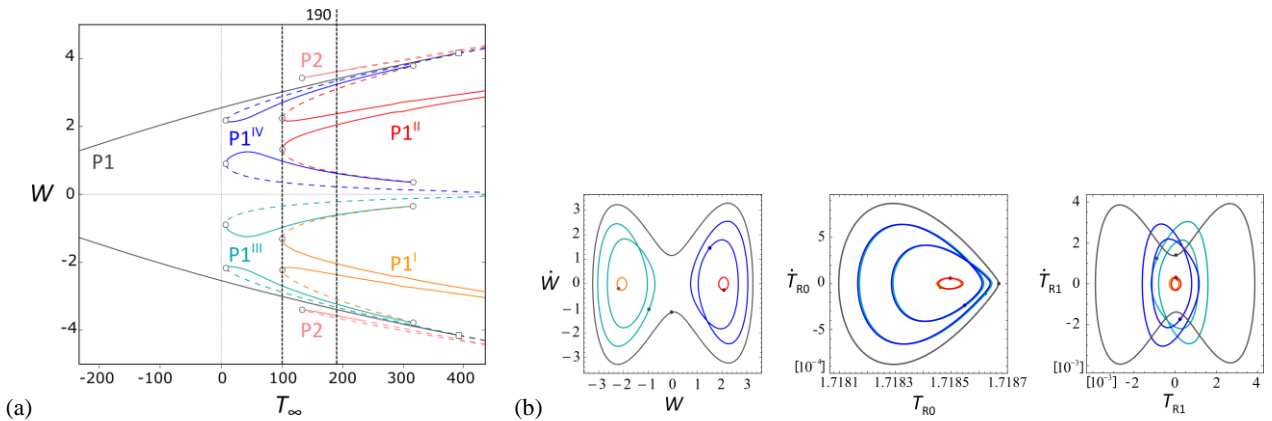


Fig 16. FHE. (a) Bifurcation diagram of transversal displacement of the plate center with varying temperature difference between plate and environment T_∞ (circle: saddle-node bifurcation, square: transcritical bifurcation; continuous lines: stable branches; dashed lines: unstable branches); (b) phase portraits of periodic solutions at $T_\infty = 190$ K. Gray P1: pre-buckling/cross-well 1-period solution; orange P1^I/red P1^{II}: buckled low-amplitude 1-period solutions; cyan P1^{III}/blue P1^{IV}: buckled high-amplitude 1-period solutions; pink P2: 2-period solutions.

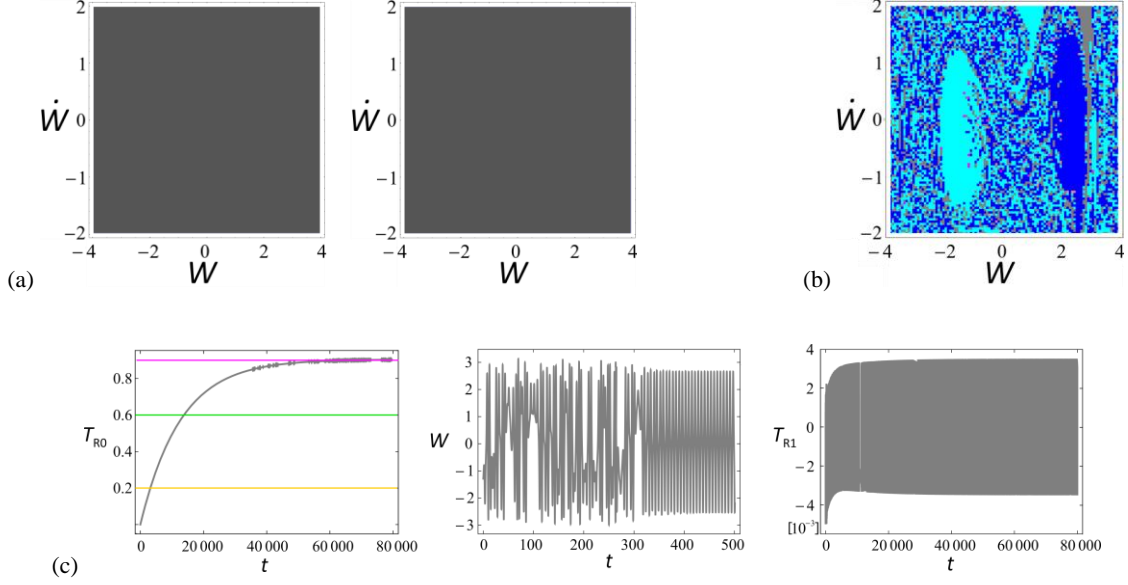


Fig 17. FHE. (a) Cross sections of 4D basin of attraction of thermomechanical model in (W, \dot{W}) plane, for $T_{R0}(0)=T_{R1}(0)=0$: (i) pre-buckling ($T_\infty = 0 K$), (ii) post-buckling ($T_\infty = 100 K$). (b) Basins of attraction of uncoupled mechanical oscillator for $T_{R0}=0.9$. (c) Time histories of thermomechanical variables, for $T_\infty = 100 K$, with i.c. $(-1.35, 0.18, 0, 0)$. (Gray P1, cyan P1^{III}, blue P1^{IV}, pink P2 basins correspond to solutions of Fig. 16; T_{R0} time history: orange, green, red horizontal lines refer to cross sections in Fig. 18).

and ensuing from the P1 pre-buckling solution which remains stable is also reported. The mechanical response is globally symmetric with respect to trivial equilibrium, yet with mirrored solutions of each couple and a radial symmetry of the respective Poincaré points (left panel of Fig. 16(b)). In turn, membrane thermal responses in each of the two couples are self-symmetric and oscillate around the mean steady state value $T_{R0} = 1.718$ (mid panel), whereas the corresponding bending responses are also mirrored with radial symmetry, as the mechanical ones from which they are dragged, and oscillate around the rest position (right panel).

To get a comprehensive understanding of the plate thermomechanical response, the local dynamics description provided by bifurcation diagrams and phase portraits/Poincaré maps is complemented with the analysis of global dynamics through basins of attraction, which provide fundamental information on the effect of initial conditions. To this aim, a lower warming ($T_\infty = 100 K$) of the environment marking the maximum interval of occurrence of the sole first couple (P1^{III}/P1^{IV}) of buckled solutions (red arrow in Fig. 16(a)) is considered, so to have a less involved topological scenario of the 4D basin of attraction (in the four, i.e. displacement, velocity, membrane and bending temperatures, state space) even though only relevant planar cross sections are constructed. Being mainly interested in grasping the influence of thermal excitations on the mechanical response, the most natural physical cross section is the one in the mechanical state plane for trivial values of thermal initial conditions, i.e. $T_{R0}(0) = T_{R1}(0) = 0$. It is shown in Fig. 17(a) for $T_\infty = 0 K$ ((i), pre-buckling) and $T_\infty = 100 K$ ((ii), post-buckling), respectively, both panels showing the presence of the sole (gray) basin of pre-buckling P1 solution, the latter scenario being inconsistent with the mixed (buckled and un-buckled) steady response pattern highlighted by the local analysis in Fig. 16. The 2D basin of attraction obtained for the ‘uncoupled’ model is also reported in Fig. 17(b). It is obtained by independently solving the uncoupled (i.e., with $a_{24} = 0$) membrane thermal equation (as per the analysis in Sect. 4.2) and then, sequentially, the mechanical equation with the ensuing mean steady value ($T_{R0} = 0.9$) of membrane temperature. A multistable scenario including the first pair of buckled solutions (P1^{III}/P1^{IV}) coexisting with the pre-buckling P1 response is obtained, consistent with the local analysis outcomes in Fig. 16.

The apparent discrepancy between Figs. 17(a(ii)) and 17(b) is explained by looking at the transient dynamics, shown in Fig. 17(c) in terms of time histories of the three reduced variables. The long transient

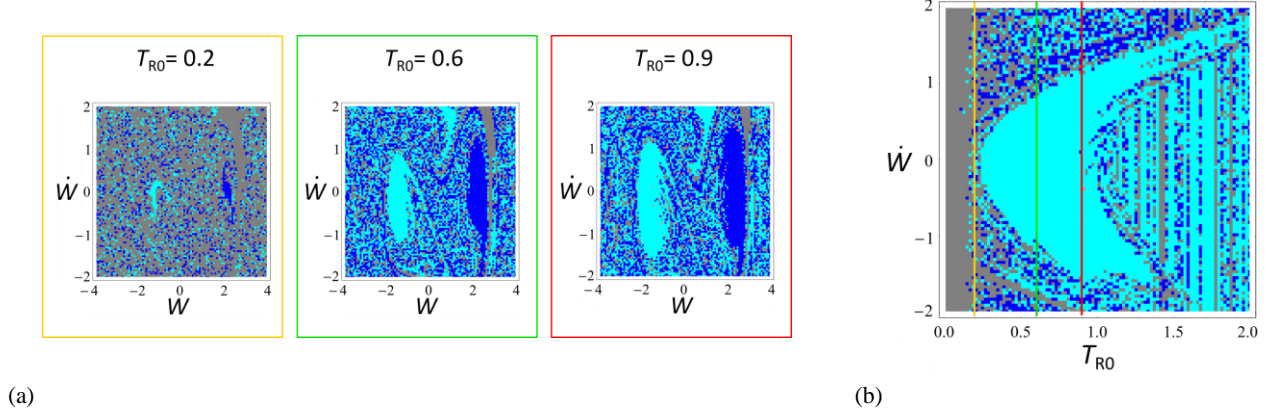


Fig 18. FHE: $T_\infty = 100 K$. (a) Cross sections of 4D basin in (W, \dot{W}) plane for increasing T_{RO} values, with $T_{R1} = 0$; (b) cross section in (T_{RO}, \dot{W}) plane for trivial T_{R1} and $W = -1.5$, with the (orange, green, red) vertical lines corresponding to mechanical cross sections in (a). Gray P1, cyan P1^{III}, blue P1^{IV}, pink P2 basins correspond to solutions of Fig. 16.

time needed by the membrane temperature to attain its steady value entails a slow thermal contribution to the mechanical stiffness responsible for buckling occurrence. As a consequence, the mechanical response, which has a much quicker dynamics, settles at the first steps of its temporal evolution to the sole stable solution depicted by the system in the pre-buckling regime, i.e. the P1 gray solution. Since this represents a robust attractor also in the post-buckling scenario, the trajectories settled onto it do not modify their behaviour when the thermal evolution is completed, with the whole contribution furnished to the mechanical stiffness. Indeed, the apparent incongruity between local and global results for the coupled model is explained by reminding that Fig. 17(a) represents just planar sections of the 4D basin, obtained for null thermal initial conditions. Considering mechanical cross sections for increasing values of T_{RO} allows us to describe the evolution of basins spatial organization (Fig. 18(a)), up to exactly reproducing the uncoupled model scenario when T_{RO} is set to the relevant mean steady value 0.9 (third panel in Fig. 18(a)). This behaviour is summarized in a different cross section of the 4D basin of attraction, i.e. the (T_{RO}, \dot{W}) plane for trivial T_{R1} in Fig. 18(b), obtained by fixing $W = -1.3$ within the buckled P1^{III} cyan basin at $T_{RO} = 0.2$ (first panel in Fig. 18(a)). Figure 18(b) shows how for $T_{RO} < 0.2$ the basin of attraction of the coupled system in the mechanical state plane coincides with the sole pre-buckling solution basin, while the buckled cyan basin appears in the (T_{RO}, \dot{W}) section and enlarges its compact part for $0.2 < T_{RO} < 0.9$. In terms of steady mechanical outcome this means that, if considering a vanishing i.c. for T_{RO} – as somehow natural from the practical viewpoint – or even a nearly vanishing one within the grey stripe ($T_{RO} < 0.2$) in the cross section of Fig. 18(b), the coupled system ends up to the pre-buckling solution. Instead, assuming $0.2 < T_{RO} < 0.9$, it is progressively much more likely to end up to the buckled solution P1^{III}, or even to the companion buckled P1^{IV} if looking at the upper/lower fractal zones in Fig. 18(b), which for $T_{RO} > 0.9$ spread over about the whole \dot{W} interval, thus making the final outcome quite uncertain.

Overall, the coupled model shows itself capable of capturing the actual, transient and steady, thermomechanical behaviour of the physical system, whose steady mechanical outcome is meaningfully affected by the slow thermal transient evolution, and also, though to a definitely minor extent, by the small thermal fluctuations actually occurring in the steady dynamics. In contrast, the uncoupled model is able to describe only the specific mechanical condition attained at the very end of the thermal transient.

It is worth noting that if a body thermal source e_0 constant along the thickness were considered, instead of the T_∞ difference with the environment, overall comparable effects would be obtained as regards local and global dynamics, although the specific response features would be generally different due to the different physical processes activated by the body vs boundary excitation [46].

Bending body source. A time constant bending excitation e_1 with linear variation along the thickness produces equal cooling and warming of the two external surfaces. The bifurcation diagram of mechanical response with varying e_1 is reported in Fig. 19(a). Moving again from a mechanically-induced pre-buckling configuration for

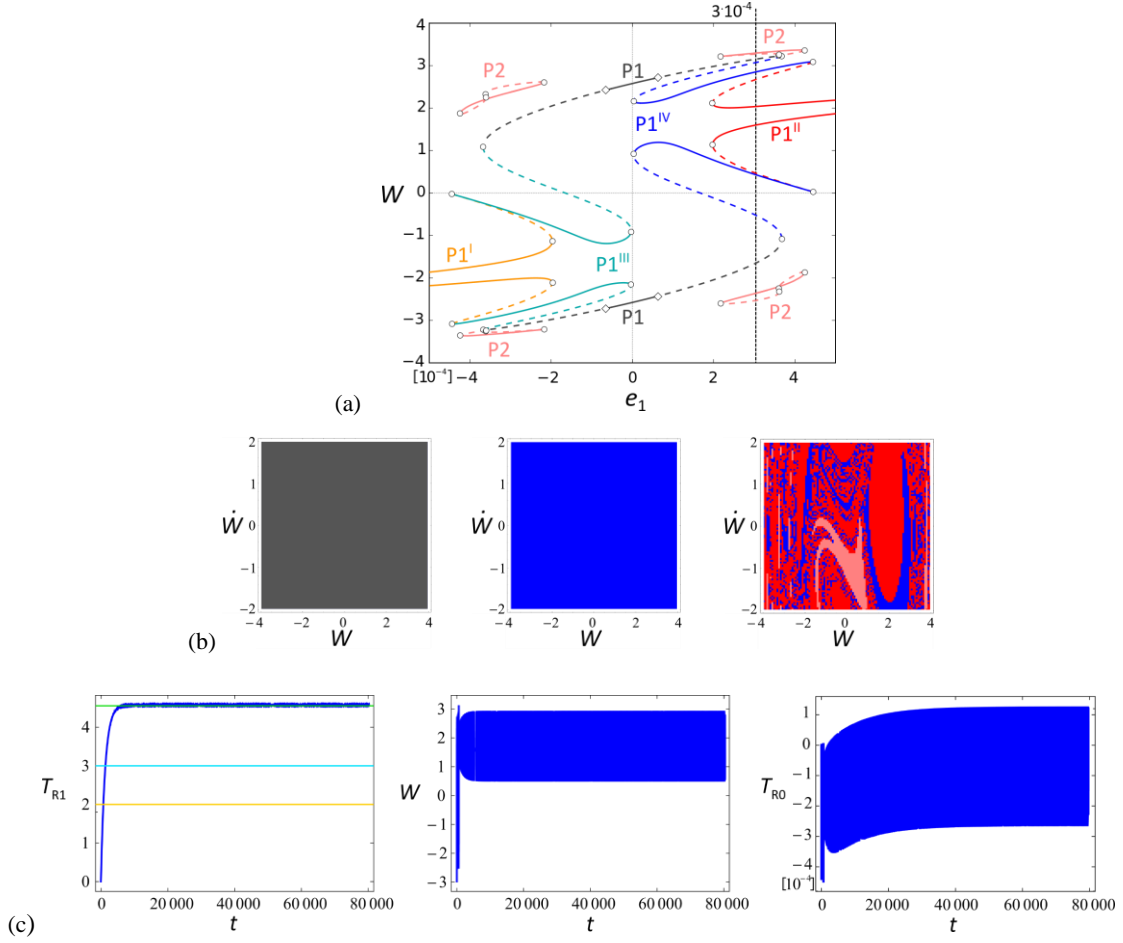


Fig 19. Bending body source. (a) Bifurcation diagram of transversal displacement of the plate center with varying bending body source e_1 (circle: saddle-node bifurcation, diamond: period-doubling bifurcation; continuous lines: stable branches; dashed lines: unstable branches). (b) Cross sections of 4D basin of attraction of thermomechanical model in (W, \dot{W}) plane, for $T_{R0}(0) = T_{R1}(0) = 0$: (i) pre-buckling ($e_1 = 0$), (ii) post-buckling ($e_1 = 0.0003$). (c) Basins of attraction of uncoupled mechanical oscillator for $T_{R1} = 4.57$. (d) Time histories of thermomechanical variables for $e_1 = 0.0003$, with i.c. $(0, 0, 0, 0)$. (Gray P1: pre-buckling/cross-well 1-period solution (basin); orange P1^I/red P1^{II}: buckled low-amplitude 1-period solutions (basins); cyan P1^{III}/blue P1^{IV}: buckled high-amplitude 1-period solutions (basins); pink P2: 2-period solutions (basins). T_{R1} time history: orange, cyan, green horizontal lines refer to cross sections in Fig. 20).

$e_1 = 0$, in which the sole one-period response P1 exists, the addition of a bending excitation generates buckled responses confined around only one positive/negative equilibrium (i.e., in one of the two potential wells, in global dynamics terms), depending on the sign of e_1 , whose change provides an overall antisymmetric scenario of mechanical response. In particular, in a range of relatively high positive values of e_1 , both the low- (P1^{II} red curve) and high- (P1^{IV} blue curve) amplitude buckled solutions exist and are stable, along with a cross-well period-2 solution P2 (pink curve) confined in a limited excitation range. However, the results obtained in terms of cross section of the 4D basin for $e_1 = 0.0003$ (ii), reported in Fig. 19(b) together with the cross section for $e_1 = 0$ (i), provide discordant indications with respect to those furnished by the bifurcation diagrams. Indeed, a monostable behavior characterized by the sole (blue) high-amplitude buckled solution P1^{IV} is observed, with no evidence of the expected basins of the (red) low-amplitude buckled solution P1^{II} and of the (pink) P2 response. Moreover, the comparison with the outcomes of the uncoupled oscillator with mean steady value $T_{R1} = 4.57$ (as deduced by the time history of the bending thermal variable in Fig. 19(d)), reported in Fig. 19(c), points out meaningful differences as regards the kind of detected solutions in the mechanical state plane. As in the previous FHE case, the reasons for this disagreement stand in the effect of the thermomechanical coupling together with the simultaneous presence of slow and fast dynamics. Indeed, the slowness of the

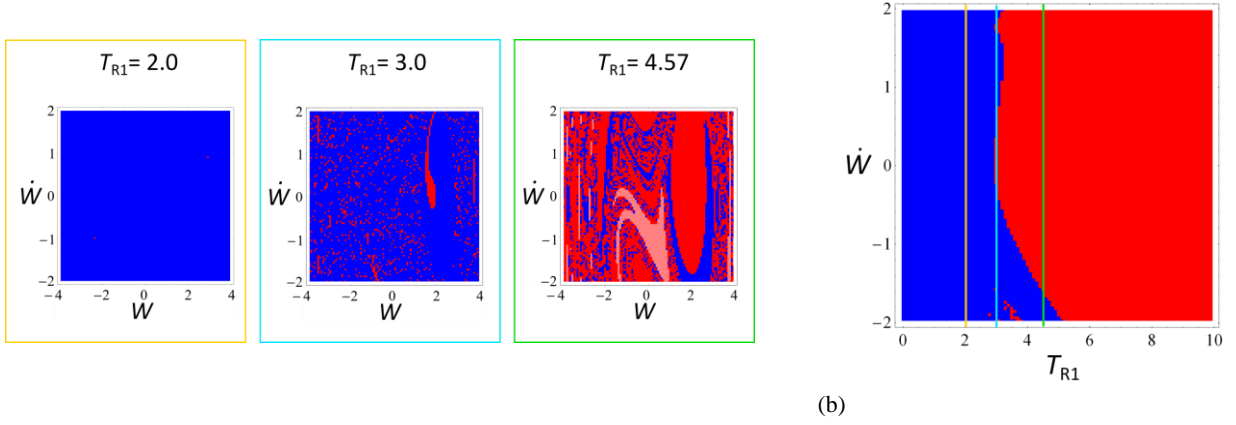


Fig 20. Bending body source: $e_1 = 0.0003$. (a) Cross sections of 4D basin in (W, \dot{W}) plane for increasing T_{R1} values, with $T_{R0} = 0$; (b) cross section in (T_{R1}, \dot{W}) plane for trivial T_{R0} , with the (orange, cyan, green) vertical lines corresponding to mechanical cross sections in (a). Red P1^{II}, blue P1^{IV}, pink P2 basins correspond to solutions of Fig. 19.

bending thermal transient (left panel of Fig. 19(d)) causes the contribution of the e_1 excitation to be supplied gradually into the mechanical equation by means of the coupling term related to T_{R1} . On the other hand, the mechanical vibration is much faster than the thermal one and its transient, needed for reaching a stable solution, is very short. From a phenomenological viewpoint, it appears possible to neglect the mechanical transient and to look only at the attractor of the system, whose evolution with increasing values of the thermal bending excitation from zero to the selected value $e_1 = 0.0003$ can be followed in the bifurcation diagram of Fig. 19(a). For low values of e_1 , where the gray P1 attractor is stable, the mechanical response is cross well at least in its first initial steps, before possibly jumping to the coexisting blue buckled solution P1^{IV} upon its onset. But when the bending excitation reaches a value ($e_1 \approx 0.000056$) providing a bending thermal variable T_{R1} in the mechanical equation such to destabilize the P1 response via a period doubling bifurcation (Fig. 19(a)), the mechanical trajectories are more likely to swiftly jump onto the P1^{IV} buckled response, as shown in the very first steps of the W time history (mid panel in Fig. 19(d)). And since this solution is stable after the rise of the further (red) buckled solution P1^{II}, the system response remains steady on it for all considered values of mechanical initial conditions.

Also in this case, considering cross sections of the 4D basin of attraction with different values of the governing thermal variable T_{R1} allows to obtain a comprehensive description of the system global dynamics. With reference to the excitation value $e_1 = 0.0003$, and looking at the final outcomes of the dynamics beginning with the given T_{R1} initial conditions, Figure 20(a) points out that relevant increasing values succeed in progressively shortening the transient dynamics and more swiftly reproducing the response of the uncoupled system when the i.c. is set to the steady value, thus capturing the presence of other basins of attraction (third vs first panel in Fig. 20(a)). As in the FHE case, the whole behaviour is summarized in Figure 20(b), which shows a cross section of the 4D basin of attraction in the (T_{R1}, \dot{W}) state plane, obtained by fixing the mechanical initial condition to $W = 1.75$, within the buckled P1^{II} red basin at $T_{R1} = 3$ (mid panel in Fig. 20(a)).

For initial $T_{R1} < 3$, the response of the coupled model always settles on the high-amplitude buckled P1^{IV} blue basin, due to the slow thermal contribution into the mechanical equation which is insufficient to move the response towards the other, yet existing, P2 and P1^{II} attractors. For $3 < T_{R1} < 5$, the arise and enlargement of the low-amplitude P1^{II} red basin is highlighted, while for high T_{R1} initial conditions the latter becomes the only existing solution for the system, according to the outcomes of the bifurcation diagrams of Fig. 19(a) showing the P1^{II} response as the only possible one for high thermal excitation. In fact, setting a high T_{R1} initial condition corresponds to provide, in the first step of the dynamical evolution, a high contribution into the mechanical equation by means of the coupling term related to a_{15} . As a consequence, the displacement response is initially moved into the monostable range characterized by the P1^{II} solution, which therefore attracts all the trajectories regardless of the chosen initial velocity. Due to the fact that such solution is stable also when the thermal

variable stabilizes around its steady value, it represents the only possible response of the system in the considered T_{R1} range. As a final comment, it is worth noting that, contrary to Fig. 18(b) of the previous FHE case, no fractal arrangement is present in Fig. 20(b), due to the different kind of mechanical buckling (symmetric versus antisymmetric) achievable with the two thermal excitations. When the membrane variable is activated, in fact, the coexistence of several buckled solutions possibly reachable by the trajectories causes the fractalization of the relevant basins, whereas the antisymmetric behaviour of the bending variable strongly reduces the multistability region and the basins are organized in a more compact way.

Constant vs dome-shaped prescribed temperatures. Contrary to FHE, arbitrary temperature values prescribed on the upper and lower surfaces generate a nonsymmetric thermal field along the thickness. Moreover, with respect to FHE which entails also convection, the involved pure conduction causes an increase of all coefficients in the second set of thermal equations of Fig. 15, and a given, pure mechanical excitation produces higher thermal responses due to the greater mechanical coupling terms a_{24} and a_{33} . Moving again from a p -induced pre-buckling configuration in which the sole P1 response exists, mechanical bifurcation diagrams in terms of PPC (black) or PPD (red) temperature on the lower surface T_{down} are compared in Fig. 21, for the fixed $T_{up} = 100 K$ value implying onset of the two high-amplitude buckled responses P1^{III} and P1^{IV}. Both mechanical responses are nonsymmetric due to the contemporary activation of membrane and bending thermal dynamics, with also a different behavior inside the positive and negative buckled wells as regards stability ranges and amplitudes of the associated P1^I/P1^{II} and P1^{III}/P1^{IV} periodic responses. The outcomes point out differences of amplitude and stability regions between PPC and PPD buckled responses for high values of T_{down} , and mostly located in the negative buckled well, which corresponds to the mechanical configuration bent towards the colder (i.e., upper) surface. Another important difference between PPC and PPD solutions occurs in the pre-buckling scenario. In fact, for negative T_{down} values, no stable periodic response occurs with PPC, whereas the negative high-amplitude buckled response P1^{III} with PPD remains stable in the whole T_{down} -negative range.

Global features of the response obtained with the two sets of b.c. are compared in Fig. 22, which reports cross sections of the corresponding 4D basins of attractions in the mechanical state plane obtained for thermal variable values set at the beginning (i.e., $T_{R0}(0) = T_{R1}(0) = 0$; left panel) and the end (i.e., $T_{R0}(0), T_{R1}(0)$ equal to steady values; right panel) of the relevant transient dynamics. Cross sections at four different T_{down} values, as per the four vertical lines in Fig. 21, are reported. For each considered T_{down} , the global response scenarios in the cross section for steady temperatures values (right panel) are fully consistent with the (steady) mechanical responses in the corresponding local bifurcation diagrams (Fig. 21). By way of example, for

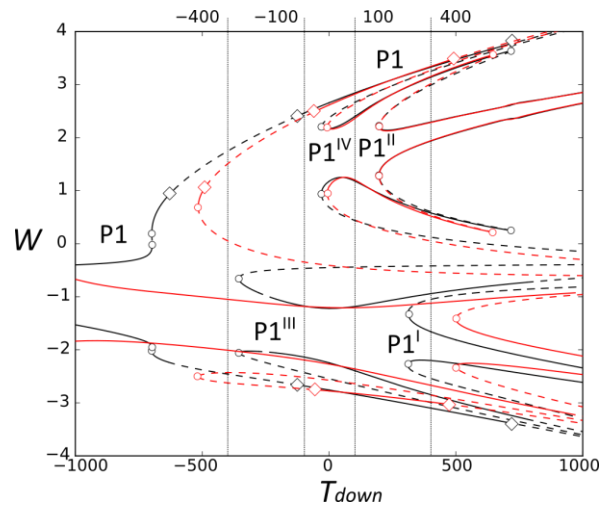


Fig 21. Bifurcation diagrams of transversal displacement of the plate center with varying temperature on the lower surface T_{down} for PPC (black) and PPD (red) boundary conditions, with temperature on the upper surface $T_{up} = 100 K$ (circle: saddle-node bifurcation, diamond: period-doubling bifurcation; continuous lines: stable branches; dashed lines: unstable branches).

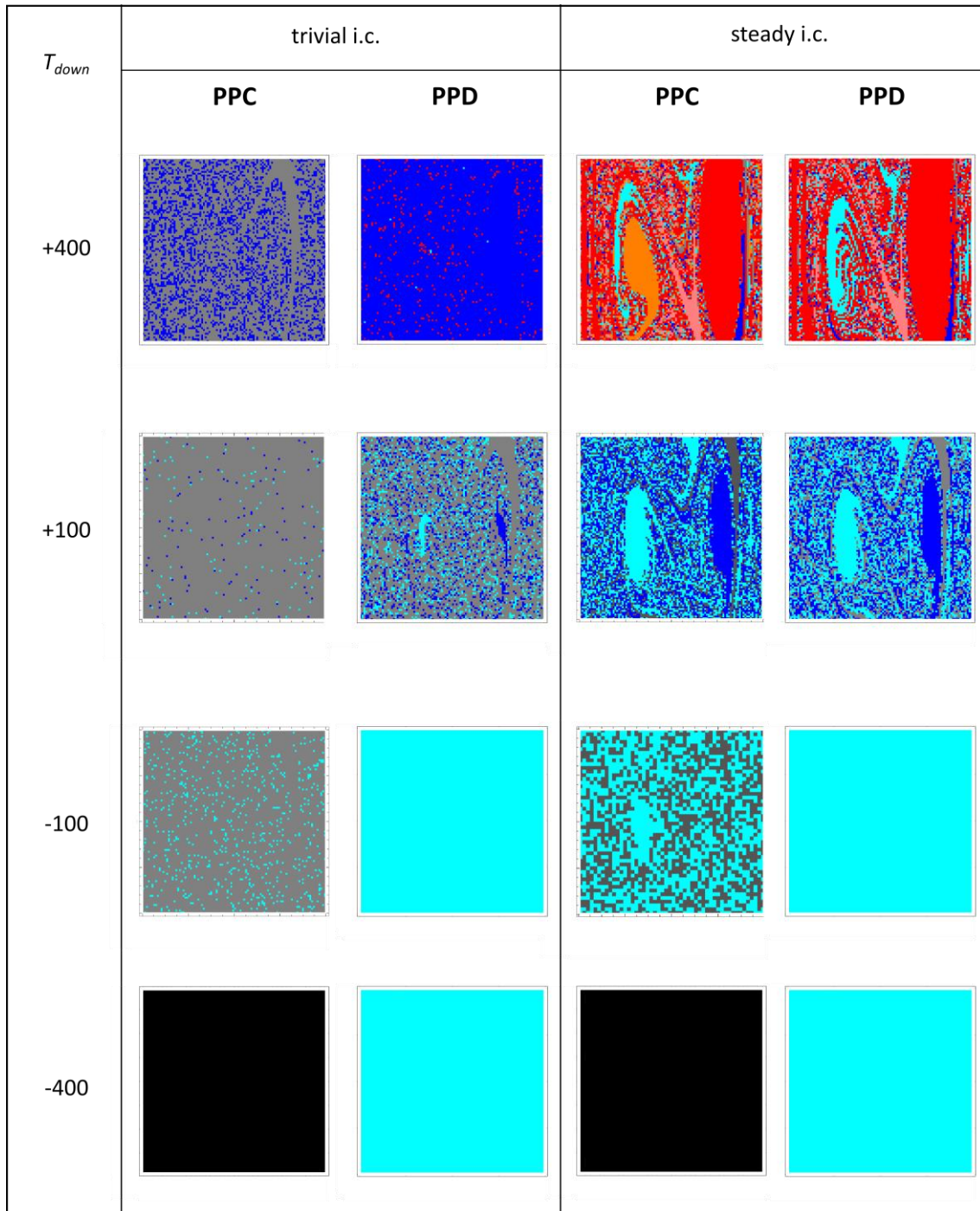


Fig 22. Cross sections of 4D basin in $(W \in [-4,4], \dot{W} \in [-2,2])$ plane at different T_{down} values and $T_{up} = 100 K$, for PPC and PPD boundary conditions, with trivial (left panel) and steady (right panel) initial values of thermal variables T_{R0} and T_{R1} . (Basins: gray P1, orange P1^I, red P1^{II}, cyan P1^{III}, blue P1^{IV}, pink P2, black chaos).

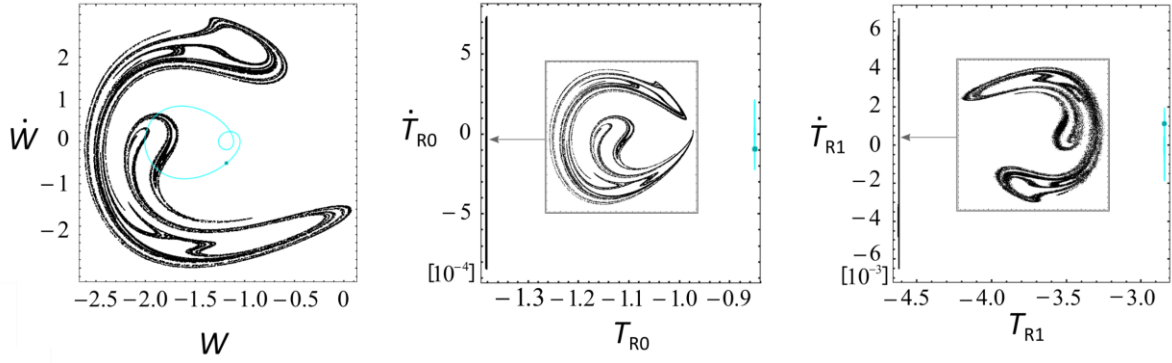


Fig 23. Phase portraits of PPC chaotic (black) and PPD periodic (cyan) solutions, at $T_{down} = -400 K$ (left vertical line in Fig. 21), with enlargements of the thermal PPC solutions highlighting the chaotic nature of the responses.

$T_{down}=400 K$, the large red basin of the low-amplitude $P1^{II}$ solution fills most of the positive buckled well with both PPC and PPD b.c., but the large orange basin of the low-amplitude $P1^I$ solution in the negative buckled well of PPC is widely replaced, with increased fractality, by the cyan basin of the high-amplitude $P1^{III}$ response of PPD, the other minor basins (of high-amplitude blue solution $P1^{IV}$, and cross-well gray P1 and pink P2 solutions) being similar with the two b.c. Meaningful qualitative differences between PPC and PPD steady cross sections occur at $T_{down} = -100 K$ and $T_{down} = -400 K$, too. In both cases, PPD b.c. entail a monostable cyan cross section, as per the corresponding solely stable $P1^{III}$ buckled (red) response in Fig. 21, whereas the PPD cross section is bistable (with nearly equivalent P1 gray and $P1^{III}$ cyan areas) at $T_{down} = -100 K$ and monostable at $T_{down} = -400 K$. However, the latter monostability (black) corresponds to a chaotic buckled solution (of purely mechanical origin) occurring for negative T_{down} values in the unstable region of the PPC bifurcation diagram, which is completely different from the $P1^{III}$ solution of PPD: the two (PPC black chaotic and PPD cyan periodic) responses are compared in the (partially zoomed) phase portraits of Fig. 23 for all three (mechanical and thermal) variables.

Cross sections of the 4D basins for trivial values of the thermal variables (left panel in Fig. 22) coincide with those for corresponding steady values (right panel) only in the case of monostable steady solutions. If the steady scenario is multistable, as for positive T_{down} values in the bifurcation diagram (Fig. 21), trivial cross sections of both PPC and PPD may strongly differ from the corresponding steady ones. As for the FHE and body bending cases in Figs. 18 and 20, respectively, this is a consequence of the variably slow thermal transient not having come into play yet, thus allowing the fast mechanical response to settle onto a different stable and more robust solution in the first instants of its time evolution, for most initial conditions. In any case, the generally different (multi- or mono-stable) response scenarios of PPC and PPD trivial cross sections (Fig. 22, left panel) entail swiftly attained mechanical steady outcomes which may be meaningfully different from each other, as highlighted, e.g., in Fig. 24(a) for $T_{down} = 400 K$ and fully trivial i.c.: the PPC response settles onto the cross-well P1 solution (black), whereas the PPD one settles onto the buckled $P1^{IV}$ solution (red).

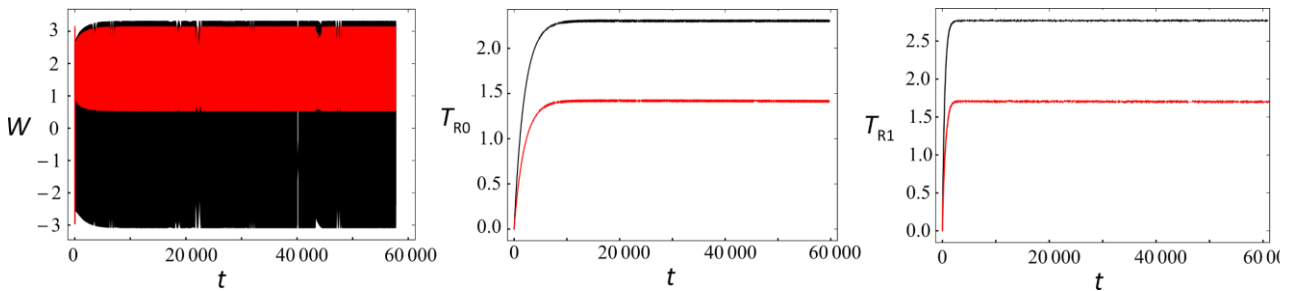


Fig 24. Time histories of P1 (black, PPC) and $P1^{IV}$ (red, PPD) solutions, with i.c. (0,0,0,0), at $T_{down} = 400 K$ (right vertical line in Fig. 21).

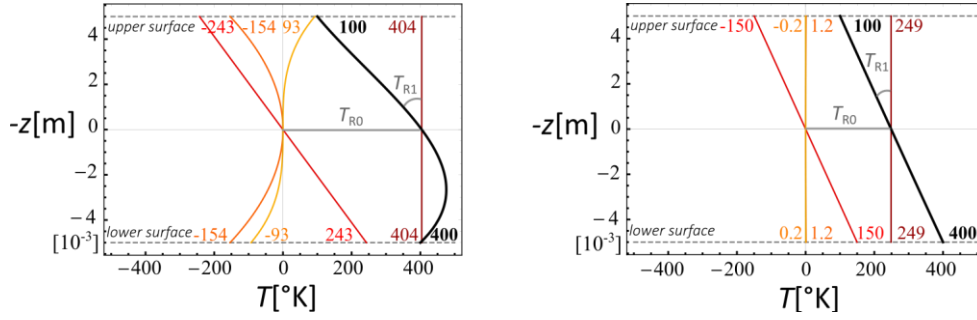


Fig 25. Temperature evolution (thick black) along the thickness in the center of the plate, and single constant (dark red), linear (red), quadratic (orange) and cubic (yellow) contributions at $T_{up} = 100 K$, $T_{down} = 400 K$, for PPC (left) and PPD (right).

As regards companion thermal variables, notwithstanding a nearly comparable length of PPC and PPD transients, steady values of the former are considerably higher than those of the latter for both T_{R0} and T_{R1} . The underlying reason for such higher values is the already mentioned inconsistency of the constant temperature prescription over the plate external surfaces of PPC with respect to the dome-shape spatial distribution of the two thermal variables over the midplane, assumed in the modeling stage (Eq. 18(d,e)). This discrepancy enforces an overestimation along the whole thickness, and thus also in the center of the plate, of the PPC thermal field resulting from the superposition of all (constant, linear, quadratic, cubic) contributions in Eq. 3 (Fig. 25, left), which is needed to satisfy the temperature values ($T_{up} = 100 K$, $T_{down} = 400 K$) prescribed on the two surfaces and to concurrently assume an internal dome-shape distribution. This does not occur for the PPD case with coherent external/internal temperature distributions, whose thermal field along the thickness (Fig. 25, right) results from the superposition of the major constant and linear contributions in Eq. 3.

Antisymmetric boundary condition vs body source. It is worth comparing the dynamics obtained when alternatively applying a prescribed boundary condition or a thermally equivalent body source. Response scenarios provided by two purely antisymmetric excitations are referred to, namely the already considered bending body source e_1 and PPD b.c. with equal and opposite values ($T_{up} = -T_{down}$), whose thermal equivalence is established by the relation $e_1 = a_{35}\alpha_1(T_{up} - T_{down})/a_{34}$ obtained from the steady uncoupled bending equation of the second set in Fig. 15. Mechanical bifurcation diagrams in terms of the alternative control parameters e_1 (blue) and $T_{up} = -T_{down}$ (red) are presented in Fig. 26(a). Despite the overall equivalent thermal effects of the two excitations, different mechanical responses are obtained due to the peculiar structure of the reduced ODEs. In fact, the boundary condition $T_{up} = -T_{down}$ modifies the mechanical behavior not only indirectly by means of the coupling term related to a_{15} , as the e_1 excitation, but also directly acting into the mechanical equation with the a_{19} term. This implies a strengthening of the external forcing produced by the thermal condition that causes the overall mechanical buckled response to occur for lower absolute values of the applied thermal source with $T_{up} = -T_{down}$ (red) than with e_1 (blue).

This behavior is confirmed by the comparison of mechanical cross sections of the 4D basins with the two excitations in a specific antisymmetric condition. Consider $T_{up} = 100 K = -T_{down}$ (vertical line in Fig. 26(a)), for which the PPD trivial and steady cross sections, already reported in Fig. 22 (third line, second and fourth columns), highlight the monostable scenario characterized by the negative buckled cyan $P1^{III}$ response, since the cross-well $P1$ solution (top red branch in Fig. 26(a)) is unstable. The corresponding cross sections (Fig. 26(b)) with the equivalent $e_1 = -9.83 \cdot 10^{-5}$ are dominated by the stable $P1$ response (top blue branch in Fig. 26(a)), with a meaningfully increasing presence of the cyan $P1^{III}$ basin as moving from the trivial (left) to the steady (right) cross section, due to the usual thermal transient effect. The temperature evolution along the thickness is also shown (Fig. 26(c)) for the two excitations. The $T_{up} = -T_{down} = 100 K$ b.c. produce a linear temperature distribution (left), whereas the equivalent body source e_1 produces a nonlinear distribution (right). Equal values of T_{R1} (i.e., the profile slope in the center) occur with the two excitations, as per the imposed

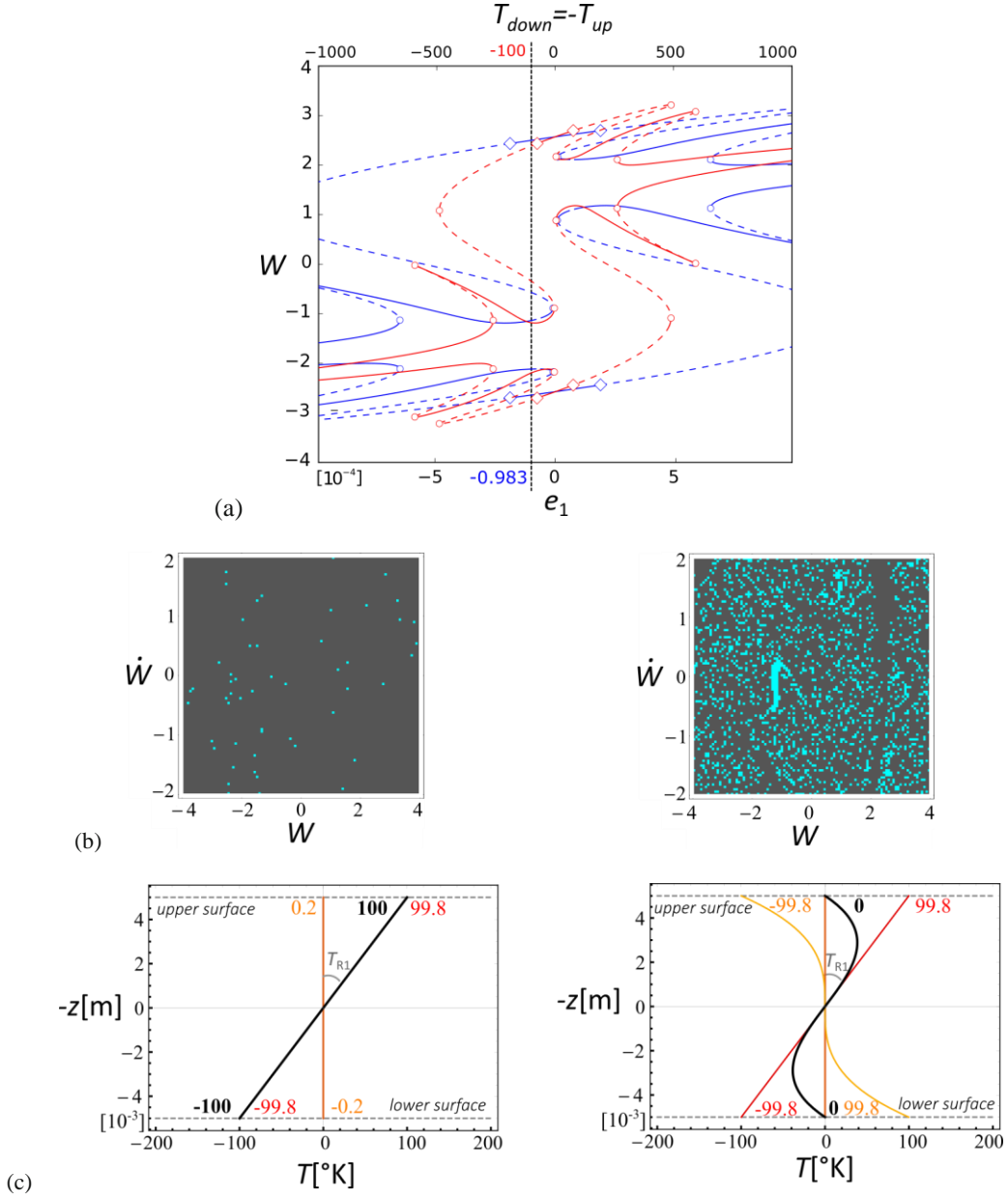


Fig 26. (a) Bifurcation diagrams of transversal displacement of the plate center with varying bending body source e_1 (blue) or prescribed temperature on the plate surfaces $T_{up} = -T_{down}$ (red) (circle: saddle-node bifurcation, diamond: period-doubling bifurcation; continuous lines: stable branches; dashed lines: unstable branches). (b) Cross sections of 4D basin in (W, \dot{W}) plane with $e_1 = -9.83 \cdot 10^{-5}$, for trivial (left) and steady ($T_{R0} = 0$, $T_{R1} = -1.138$, right) initial values of thermal variables T_{R0} and T_{R1} . (Basins: gray P1, cyan P1^{III}). (c) Temperature evolution (thick black) along the thickness in the center of the plate, and single linear (red) and cubic (yellow) contributions for $T_{up} = -T_{down} = 100$ K (left) and $e_1 = -9.83 \cdot 10^{-5}$ (right).

bending equivalence. However, when applying the sole body source, temperature values are implicitly set to zero on the upper and lower surfaces (otherwise non-vanishing $T_{up} = -T_{down}$ contributions would exist in all equations), thus entailing the antisymmetric temperature profile along the thickness to settle to a cubic shape.

6. Effect of thermomechanical coupling

After presenting the local and global dynamics of the fully coupled TTC model subjected to mechanical excitation and a variety of thermal excitations, it is worth resuming the issue of which response features would

$\begin{aligned} \dot{W}(t) + a_{12}\dot{W}(t) + a_{13}W(t) + a_{14}W(t)^3 + a_{15}T_{R1}(t) + a_{16}T_{R0}(t)W(t) + a_{17}\text{Cos}(t) &= 0 \\ \dot{T}_{R0}(t) + a_{22}T_{R0}(t) + a_{23}\alpha_1 T_\infty + a_{24}W(t)\dot{W}(t) + a_{25}e_0(t) &= 0 \\ \dot{T}_{R1}(t) + a_{32}T_{R1}(t) + a_{33}\dot{W}(t) + a_{34}e_1(t) &= 0 \end{aligned}$	<p>3-dof two-way (fully) coupled: 3-2 model</p>
$\begin{aligned} \dot{W}(t) + a_{12}\dot{W}(t) + a_{13}W(t) + a_{14}W(t)^3 + a_{15}T_{R1}(t) + a_{16}T_{R0}(t)W(t) + a_{17}\text{Cos}(t) &= 0 \\ \dot{T}_{R0}(t) + a_{22}T_{R0}(t) + a_{23}\alpha_1 T_\infty + a_{24}W(t)\dot{W}(t) + a_{25}e_0(t) &= 0 \\ \dot{T}_{R1}(t) + a_{32}T_{R1}(t) + a_{33}\dot{W}(t) + a_{34}e_1(t) &= 0 \end{aligned}$	<p>3-dof one-way coupled: 3-1 model</p>
$\begin{aligned} \dot{W}(t) + a_{12}\dot{W}(t) + a_{13}W(t) + a_{14}W(t)^3 + a_{15}T_{R1}(t) + a_{16}T_{R0}(t)W(t) + a_{17}\text{Cos}(t) &= 0 \\ \dot{T}_{R0}(t) + a_{22}T_{R0}(t) + a_{23}\alpha_1 T_\infty + a_{24}W(t)\dot{W}(t) + a_{25}e_0(t) &= 0 \\ \dot{T}_{R1}(t) + a_{32}T_{R1}(t) + a_{33}\dot{W}(t) + a_{34}e_1(t) &= 0 \end{aligned}$	<p>2-dof two-way coupled with only active bending equation: 2-2 model</p>
$\begin{aligned} \dot{W}(t) + a_{12}\dot{W}(t) + a_{13}W(t) + a_{14}W(t)^3 + a_{15}T_{R1}(t) + a_{16}T_{R0}(t)W(t) + a_{17}\text{Cos}(t) &= 0 \\ \dot{T}_{R0}(t) + a_{22}T_{R0}(t) + a_{23}\alpha_1 T_\infty + a_{24}W(t)\dot{W}(t) + a_{25}e_0(t) &= 0 \\ \dot{T}_{R1}(t) + a_{32}T_{R1}(t) + a_{33}\dot{W}(t) + a_{34}e_1(t) &= 0 \end{aligned}$	<p>2-dof one-way coupled with only active bending equation: 2-1 model</p>
$\begin{aligned} \dot{W}(t) + a_{12}\dot{W}(t) + a_{13}W(t) + a_{14}W(t)^3 + a_{15}T_{R1}(t) + a_{16}T_{R0}(t)W(t) + a_{17}\text{Cos}(t) &= 0 \\ \dot{T}_{R0}(t) + a_{22}T_{R0}(t) + a_{23}\alpha_1 T_\infty + a_{24}W(t)\dot{W}(t) + a_{25}e_0(t) &= 0 \\ \dot{T}_{R1}(t) + a_{32}T_{R1}(t) + a_{33}\dot{W}(t) + a_{34}e_1(t) &= 0 \end{aligned}$	<p>uncoupled mechanical model (with $T_{R1} = -a_{34}e_1/a_{32}$): 1 model</p>

Fig 27. Further reduced models: from 3-dof two-way, i.e. fully, coupled (model 3-2, top block) to mechanical uncoupled (model 1, bottom block). Intermediate models: (i) two-way coupled, with the sole active bending thermal equation/unknown (2-dof model 2-2, mid-block); one-way coupled, with no mechanical contributions into (ii) both thermal equations (3-dof model 3-1, second block from top) or (iii) the sole bending thermal equation (2-dof model 2-1, second block from bottom).

be missed or kept, if alternatively performing a partially coupled analysis or even an uncoupled one. This is made by evaluating the importance of the various terms and variables of coupling entering the full equations, as regards contributing to a satisfactory and comprehensive description of the response. Indeed, outcomes of investigations performed for different active thermal regimes have highlighted a minor role played in the mechanical response by the mechanical coupling terms in thermal equations, which govern the two-way coupling, and by the non-directly excited thermal variables/equations, which govern the number of essential thermal degrees of freedom. This provides useful hints as to a further possible dimensional reduction of the considered model. Both two-way (from thermal to mechanical, and from mechanical to thermal) and one-way (from thermal to mechanical) coupling are considered, along with intermediate models accounting for only the directly excited thermal equation/variable [46].

Reference is made to the simplest case of FHE b.c., whose first set of fully coupled equations (Fig. 15) are reported on top of Fig. 27 and referred to as **3-2** model because of including 3-dof and accounting for two-way coupling. Moving from it, a sequence of gradually simplified ROMs is obtained by neglecting coupling terms and/or equations/variables. A 3-dof one-way coupled model (from thermal to mechanical), named **3-1**, is obtained by neglecting the mechanical contribution into the thermal equations, i.e. by setting $a_{24} = a_{33} = 0$. Then, based on the kind of considered thermal excitation, a further dimension reduction to a 2-dof model can be obtained by considering only one active thermal equation/variable, since a symmetric (antisymmetric) thermal source entails a response with predominant membrane (bending) temperature field. Here, the sole body bending excitation e_1 is considered (i.e., $T_\infty = e_0 = 0$) in addition to mechanical ones, because, due to the generally high value of the a_{32}/a_{23} ratio of relevant thermal stiffnesses, it affects the mechanical response (via the a_{15} coupling term in the relevant equation) more swiftly than a membrane (T_∞ or e_0) excitation, whose equation is thus disregarded. The ensuing two-way coupled model is named **2-2** in Fig. 27. With further reductions, a 2-dof one-way model (**2-1**) is obtained by neglecting the coupling term a_{33} , ending up to the most

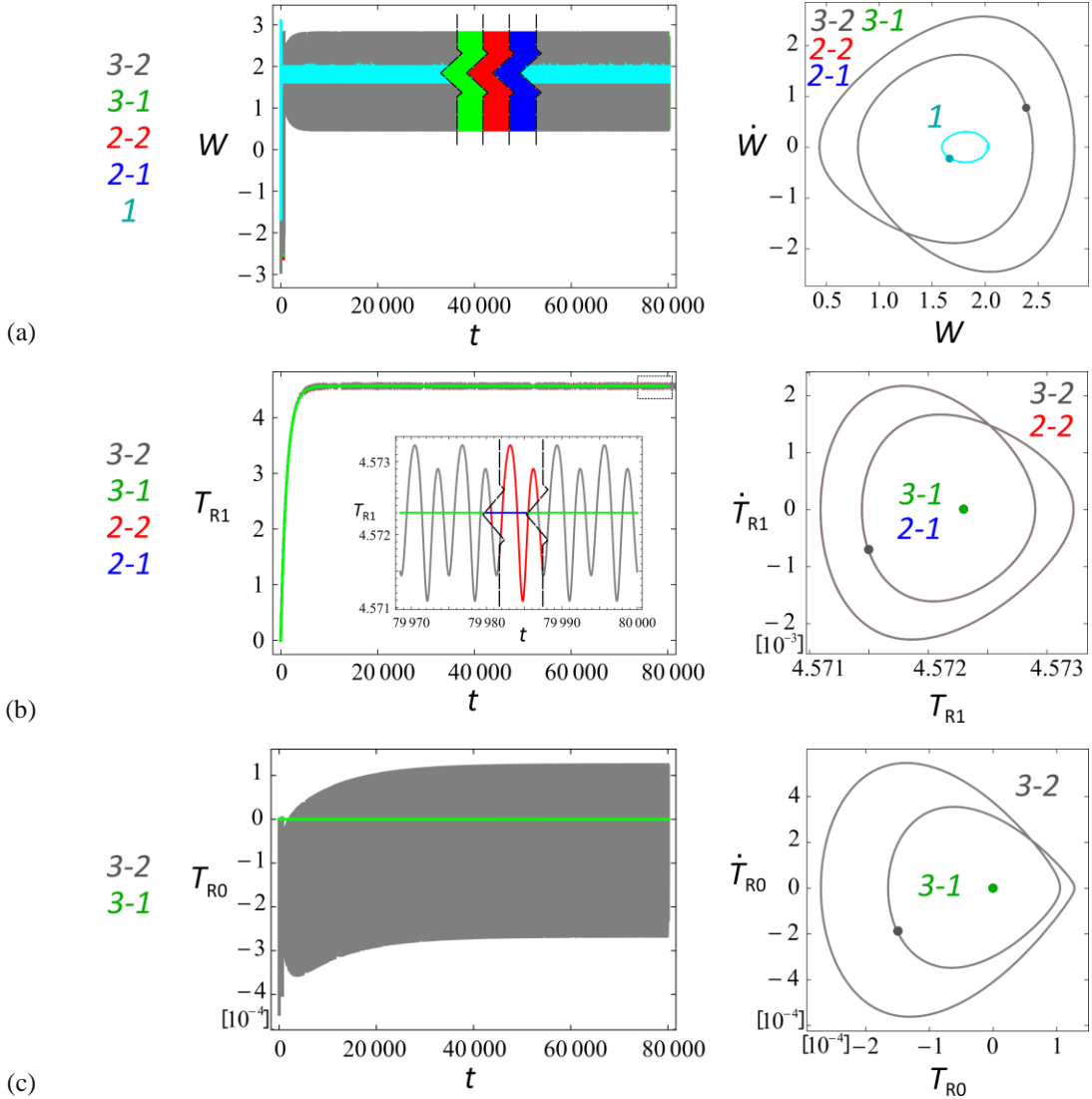


Fig 28. Time histories, phase portraits and Poincaré maps of displacement (a), bending temperature (b) and membrane temperature (c), for $e_1 = 0.0003$ and trivial i.c., with the different reduced models presented in Fig. 27.

simplified model (*I*) – already considered for comparison in previous analyses – composed of the sole mechanical equation with no membrane contribution ($a_{16} = 0$) and with bending thermal excitation taken into account by setting T_{R1} to the mean steady value $T_{R1} = -a_{34}e_1/a_{32}$ obtained from the bending equation. Local bifurcation analysis of all four, further reduced, models with varying e_1 furnishes exactly the same mechanical diagram, also equal, substantially, to that of the fully coupled **3-2** model in Fig. 19(a), highlighting how the steady periodic responses are insensitive to both the possibly different thermomechanical transient and the coupling. Instead, differences occur in the bifurcation diagrams of bending and membrane thermal variables (not shown for the sake of conciseness, see [46]). In fact, while the response of the directly activated variable T_{R1} cannot be followed by the uncoupled *I* model (although its value is known from the corresponding equation), the behavior of the dragged temperature T_{R0} can be described by the sole **3-2** and **3-1** models which include both thermal variables. Moreover, with respect to the latter, the fully coupled **3-2** model is the only one able to correctly grasp the T_{R0} response, since the 3-dof one-way model, although considering the membrane variable, furnishes identically null solutions due to the non-activation of the corresponding equation.

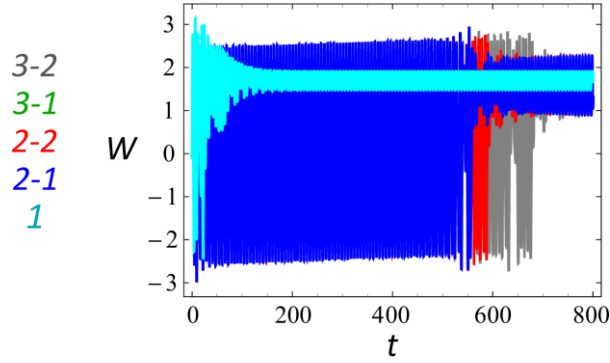


Fig 29. Transient dynamics of the mechanical response, for $e_1 = 0.0003$ and trivial i.c., with the different reduced models presented in Fig. 27.

In turn, global analysis of **3-1**, **2-2** and **2-1** models for $e_1 = 0.0003$ provides mechanical cross sections for trivial thermal initial conditions always equal to the **3-2** model cross section in Fig. 19(b(ii)) characterized by the sole (blue) buckled $P1^{IV}$ solution, different from the global scenario of the mechanical uncoupled **1** model in Fig. 19(c), which exhibits all three basins (red $P1^II$, blue $P1^{IV}$, pink $P2$) of the buckled solutions identified by the local analysis. Again, this is due to the slowness of the bending thermal transient (taken into account also by the simplified coupled models due to the combined presence of the bending equation and the a_{15} term, but ignored in the uncoupled model), that causes the contribution of e_1 to be supplied gradually into the mechanical equation via the coupling term related to T_{R1} , thus allowing the swift mechanical vibration to jump onto the persistingly stable $P1^{IV}$ buckled response (see earlier comments to the mid panel in Fig. 19(d)).

The effect of the various coupling terms is discussed further by looking at the temporal evolution of a single trajectory with fixed trivial initial conditions, as provided by the five models, along with the associated steady phase portraits and Poincaré maps (Fig. 28). The mechanical time histories of the four coupled models (non-cyan colors in Fig. 28(a)) show the swift initial jump onto the high-amplitude steady $P1^{IV}$ solution, whereas the time law of the uncoupled model **1** (cyan) jumps onto the low-amplitude steady $P1^II$, because the selected mechanical initial conditions belong to different basins of attraction (Fig. 19(b(ii),c)). Moving to the temporal evolution of thermal variables, the time histories of the directly activated bending one (Fig. 28(b)) obtained with the four coupled models allow to point out the role played by the two-way coupling. In fact, the sole gray **3-2** and red **2-2** models catch the small periodic oscillation around the steady value common to all coupled models, due to the contribution of the mechanical response via the a_{33} coupling term, while the one-way **3-1** and **2-1** models exhibit the steady equilibrium with no oscillation. The coincidence of T_{R1} outcomes for the one-way models (**3-1** \equiv **2-1**) directly ensues from the neglected a_{33} coupling term in the bending equation. In turn, the T_{R1} coincidence for also the two-way models (**3-2** \equiv **2-2**) highlights that, even in the fully coupled case (**3-2**), the membrane variable indirectly activated by e_1 , via W , entails such small (i.e., higher order) coupling effects on T_{R1} to produce an overall behavior of the latter undistinguishable from that obtained with **2-2**, where the membrane equation/variable is disregarded. Finally, the dynamics of the (though very small) dragged membrane temperature is caught only by the fully coupled **3-2** model (Fig. 28(c)), able to originate a non-null response by means of the a_{24} coupling term, while the **3-1** model also including the T_{R0} variable provides a null outcome due to non-activation of the corresponding equation.

Figure 29 compares the transient mechanical responses obtained with the five models, whose lengths are linked with neglecting or accounting for coupling terms. The mechanical cyan model **1** exhibits the shortest transient, since the whole contribution of the bending excitation to the mechanical equation is provided at the beginning of the time history. The one-way models (green **3-1** and blue **2-1**) display the same transient duration, since the membrane thermal variable T_{R0} , although being present in the **3-1** model, is not actually

activated due to the missing a_{24} coupling term, thus having no influence on the displacement evolution. Finally, the two-way models (gray **3-2** and red **2-2**) accounting for coupling terms also in thermal equations exhibit longer mechanical transients, the longest one being provided by the fully coupled **3-2** model thanks to the very slow contribution supplied by also the dragged membrane variable (Fig. 28(c)).

In the light of all the above results it appears that, with the solely considered (bending) thermal excitation, the 2-dof one-way **2-1** model is the most ‘economical’ one to be conveniently used for a systematic numerical investigation aimed at reliably describing the response in terms of the mechanical variable and of the dominant (i.e., bending) thermal one, although caught in its solely steady features. Of course, outcomes will be different if considering a combined membrane/bending thermal excitation, with the definite need to use at least the **3-1** model. Indeed, the two-way coupled model **3-2** is necessary to grasp the actual dynamic evolution in steady conditions not only of the mechanical variable but also of thermal variables.

In general terms, the model to be selected for nonlinear dynamic analysis strongly depends on the response aspects and operating conditions of interest, according to the following summary of relevant capabilities/deficiencies.

- *Two-way* coupled models (thermally complete, **3-2**, or incomplete, **2-2**)
Due to mechanical coupling in thermal equations:
 - thermal dynamics directly excited → actual time-varying steady response caught;
 - thermal dynamics non-directly (i.e. passively) excited → dragged into the response in complete model;
 - structural dynamics: very slow contributions of thermal variables (with membrane much slower than bending) entails lengthy transient response, which is longer for the complete model due to contribution of also the dragged thermal variable.
- *One-way* coupled models (thermally complete, **3-1**, or incomplete, **2-1**)
Due to missing mechanical coupling in thermal equations:
 - thermal dynamics directly excited → stationary instead of time-varying steady response;
 - thermal dynamics non-directly excited → not dragged into the response even in complete model;
 - structural dynamics: only slightly reduced transient with respect to two-way coupled models, due to missing time-varying steady response of coupled thermal variable(s) directly excited.
- *Uncoupled* thermal-mechanical model (**1**):
 - steady thermal dynamics: independently obtained by solving the mechanically-uncoupled equations;
 - steady structural dynamics: missing slow thermal transients may entail totally different structural response, depending on the relevant i.c.

7. Conclusions

Thermomechanical coupling of composite plates in a nonlinear dynamic environment is a topic of major interest in aerospace, mechanical and civil engineering, that can be addressed via a two-way (i.e., full) or one-way (i.e., partial) coupling formulation. Within the former less common, yet more general, perspective, dealing with the richness and possible complexity of the nonlinear response requires developing proper reduced order models such to exhibit the main features of the continuous problem in the background and to allow extended and detailed, but economical, parametric investigations in a variety of mechanical and thermal conditions. The wide body of research conducted in the last few years on the related modeling, analysis and phenomenology has been overviewed in this paper.

As regards the modeling stage, thermomechanical problem has been formulated in a unified way first at the two-dimensional level, by looking at the considered von Kármán model, with or without shear deformability, against a large variety of (general or approximate) nonlinear coupled models to be possibly constructed. In both the correspondingly consistent, cubic or linear, assumed distributions of temperature along the thickness, thermal field is described by sole two variables, by properly accounting for arbitrary boundary conditions prescribed on the upper and lower surfaces. Then, a consistent and controllable dimension reduction of the mechanical field has been carried out, based on two sequential kinematic condensations, of in-plane and shear

rotations dynamics, performed at the continuous and reduced level, respectively. Considering single-mode Galerkin discretization has allowed to end up to minimal models with one (transverse) mechanical and two (membrane and bending) thermal unknown variables, which still exhibit the nonlinear and full thermomechanical coupling features embedded in the underlying continuous models. In particular, the minimal ROM based on cubic assumptions for the 2D mechanical and thermal fields has allowed to deal with not only (in-plane and transverse) mechanical excitations, but also a meaningful variety of body and, mostly, boundary thermal sources.

After validating minimal ROMs in terms of linear dynamics and mechanical/thermal buckling, a first stage of numerical analysis has been concerned with the sole thermal dynamics, by reconstructing the transient and steady 3D spatiotemporal responses from the reduced models outcomes via a controllable backward procedure. Two cases of pure or mixed boundary excitations, and one case of mixed boundary/body thermal sources have been considered. Comparison with analytical solutions, with responses provided by a higher order reduced model, and with finite elements results has allowed to get a comprehensive and reliable understanding of the thermal dynamics entailed by different excitations. The minimal TTC model capable to account for a variety of excitations and thermal boundary conditions of technical interest has been identified as the ‘best’-selected minimal model in terms of richness, reliability and cheapness, to be used in the computationally demanding investigation of nonlinear/complex dynamics of symmetric cross-ply laminates.

This has been conducted by systematically analysing the local and global nonlinear dynamics of a square epoxy/carbon fiber composite plate under a variety of distinct, time-independent, thermal (boundary and body) sources entailing direct activation of the temperature field, in addition to mechanical excitations consisting of in-plane pre-stressing axial force in incipient buckling condition and transverse harmonic excitation at primary resonance. Considered thermal excitations include (i) free heat exchange with the environment, (ii) a body source entailing sole plate bending, prescribed (iii) constant or (iv) dome-shaped spatial distributions of temperature on the upper and lower surfaces, giving rise to an asymmetric transverse thermal field, and (v) a comparison of purely antisymmetric sources of different (boundary vs body) nature, thermally equivalent with each other but with different dynamical effects.

Nonlinear tools of analysis of local and global dynamics have been used in the numerical investigation, including bifurcation diagrams under varying thermal excitations, time histories, phase portraits, Poincaré maps, and planar cross sections of 4D basins of attraction. Both transient and steady responses have been summarized, providing a comparative overview of the effects of different thermal excitations on the mechanical response in pre- and post-buckling conditions, highlighting the great variety of dynamical scenarios obtainable under different (quantitative and qualitative) prescriptions for the same kind of thermal excitation, and the overall meaningful changes of dynamical responses.

In all considered cases, complex interaction phenomena characterized by the coexisting slow-fast dynamics have been unveiled by means of global dynamics. Indeed, the analysis of proper cross sections of the multidimensional basin of attraction has been seen to play a fundamental role for unveiling the important effects of the slow transient evolution of thermal response on the steady outcome of the much swifter mechanical vibrations. In particular, depending on the considered thermal initial conditions, the steady mechanical response may substantially differ from the specific one provided by the uncoupled model, which is solely able to describe the condition attained at the very end of the thermal transient, whereas the coupled model is capable to capture the entire set of transient and steady thermomechanical behaviours of the actual multiphysics system.

Still in the context of the minimal reliable, yet ‘economical’, modeling perspective, the issue of a possible further reduction of the considered ROMs has been dealt with, evaluating the importance of the various terms and variables of coupling entering the full thermomechanical equations, as regards contributing to a satisfactory and comprehensive description of the response in different (thermal) excitation conditions. A sequence of lower dimensional and/or partially coupled models has been identified, ending up to the mechanically uncoupled one with prescribed steady temperature. A summary of correctly caught or missing thermal and mechanical outcomes, obtainable by considering two- or one-way coupled models, or the

uncoupled one, has been presented, pointing out how the proper selection of a reliable model for nonlinear dynamic analysis strongly depends on the response aspects and operating conditions of interest.

The issue of the two-way versus one-way comparison is subtle, and requires further investigation with both strongly reduced and large order models. Yet, the accomplished comparative analysis of minimal ROM responses to one exemplary excitation has allowed to highlight the effects of considering or neglecting specific coupling terms, and to draw a tentative overall picture of expectable qualitative outcomes under more general excitation conditions. As regards structural response, missing mechanical couplings in thermal equations entail relatively minor changes with respect to the two-way model, mostly due to the reduced importance of the thermal transients. In this respect, irrespective of its simplicity, the considered minimal ROM furnishes just the same general outcome of an overall appropriateness of the one-way coupling as obtained in the literature by richer (and certainly more precise) models. As regards thermal response, major differences between two-way and one-way coupled models can be expected, linked with the associated time-varying vs stationary response regimes, with the considered thermal variables/conditions and, possibly, with other aspects. Finally, the reliability of uncoupled analyses strongly depends on the possibly minor importance of the overlooked thermal transient in a given application area.

Of course, the presented reduced modeling framework is not proposed as an alternative to multi-dof (finite element) models to be adopted in most engineering applications. Yet, whether properly conceived and used, minimal models may definitely allow extended analyses and in-depth understanding of at least some fundamentals of the system nonlinear dynamics, thus representing valuable tools in the preliminary investigation stage of technical applications.

Research is currently going on as regards the asymptotic formulation of bifurcation scenarios in pre- and post-buckling regimes, by properly accounting for the different time scales on which mechanical and thermal dynamics do develop. Experimental validations are also planned. In a wider and more general multiphysics context also including, e.g., electromagnetic phenomena, the generality and controllability of the developed unified approach may be suitably exploited to formulate proper minimal ROMs for nonlinear dynamic analyses in micro/nano-engineering.

Acknowledgements The financial support of Italian research program PRIN2015 (No. 2015JW9NJT) is gratefully acknowledged.

References

1. Perez R, Wang XQ, Mignolet MP. Nonlinear reduced-order models for thermoelastodynamic response of isotropic and functionally graded panels. *AIAA J* 2011;49(3):630-41.
2. Amsallem D, Cortial J, Carlberg K, Farhat C. A method for interpolating on manifolds structural dynamics reduced-order models. *Int J Num Meth Engng* 2009;80:1241-58
3. Jain S, Tiso P. Model order reduction for temperature-dependent nonlinear mechanical systems: a multiple scales approach. *J Sound Vib* 2020;465:115022
4. Nowinski JL. Theory of thermoelasticity with applications. Vol. 3. Alphen aan den Rijn: Sijhoff & Noordhoff International Publishers; 1978.
5. Allen DH. Thermomechanical coupling in inelastic solids. *Appl Mech Rev* 1991;44(8):361-73.
6. Karagiozova D, Manoach E. Coupling effect in an elastic-plastic beam subjected to heat impact. *Nucl Eng Des* 1992; 135(3):267-76.
7. Shin ES, Kim SJ. Quantitative prediction of thermomechanical coupling effect in thermo-elasto-viscoplastic composite materials. *AIAA J* 1997; 35(11):1746-52.
8. Senchenkov K, Andrushko NF. Thermomechanical coupling effects in a materially nonlinear disk under impulsive radial loading. *Int Appl Mech* 2006; 42(8):951-58.
9. Bednarczyk BA, Aboudi J, Arnold SM, Pineda EJ. A multiscale two-way thermomechanically coupled micromechanics analysis of the impact response of thermo-elastic-viscoplastic composites. *Int J Solids Struct* 2019; 161:228-42.
10. Aboudi J, Arnold SM, Bednarczyk BA. *Micromechanics of composite materials: A generalized multiscale analysis approach*. Oxford: Elsevier; 2013.
11. Daneshjo K, Ramezani M. Classical coupled thermoelasticity in laminated composite plates based on third-order shear deformation theory. *Compos Struct* 2004; 64(3-4):369-75.
12. Lezgy-Nazargah M. Fully coupled thermo-mechanical analysis of bi-directional FGM beams using NURBS isogeometric finite element approach. *Aerosp Sci Technol* 2015; 45:154-64.
13. Brischetto S, Carrera E. Coupled thermo-mechanical analysis of one-layered and multi-layered plates. *Compos Struct* 2010; 92(8):1793-812.
14. Fazzolari FA, Carrera E. Coupled thermoelastic effect in free vibration analysis of anisotropic multilayered plates and FGM plates using a variable-kinematics Ritz formulation. *Eur J Mech A/Solids* 2014; 44:157-74.
15. Culler AJ, McNamara JJ. Studies on fluid-thermal-structural coupling for aerothermoelasticity in hypersonic flow. *AIAA J* 2010; 48(8):1721-38.
16. Culler AJ, McNamara JJ. Impact of fluid-thermal-structural coupling on response prediction of hypersonic skin panels. *AIAA J* 2011; 49(11):2393-406.
17. Goodpaster BA, Harne RL. Analytical modeling and impedance characterization of the nonlinear dynamics of thermomechanically coupled structures. *J Appl Mech* 2018; 85:081010-1-9.
18. Awrejcewicz J, Krysko VA. *Elastic and thermoelastic problems in nonlinear dynamics of structural members*. Cham: Springer Nature; 2020.
19. Krysko-Jr VA, Awrejcewicz J, Yakovleva TV, Kirichenko AV, Szymanowska O, Krysko VA. Mathematical modeling of mems elements subjected to external forces, temperature and noise, taking account of coupling of temperature and deformation fields as well as a nonhomogenous material structure. *Commun Nonlinear Sci Numer Simul* 2019; 72:39-58.
20. Lee J. Large-amplitude plate vibration in an elevated thermal environment. *Appl Mech Rev* 1993; 46(11S):S242-54.
21. Shi Y, Lee RYY, Mei C. Thermal postbuckling of composite plates using the finite element modal coordinate method. *J Therm Stress* 1999; 22(6):595-614.
22. Ribeiro P. Thermally induced transitions to chaos in plate vibrations. *J Sound Vib* 2007; 299(1-2):314-30.
23. Amabili M, Carra S. Thermal effects on geometrically nonlinear vibrations of rectangular plates with fixed edges. *J Sound Vib* 2009; 321:936-54.
24. Amabili M, Tajahmadi MRS. Thermal post-buckling of laminated and isotropic rectangular plates with fixed edges: comparison of experimental and numerical results. *Proc Inst Mech Eng Part C* 2012; 226(10):2393-401.
25. Alijani F, Bakhtiari-Nejad F, Amabili M. Nonlinear vibrations of FGM rectangular plates in thermal environments. *Nonlinear Dyn* 2011; 66(3):251-70.

26. Huang XL, Shen HS. Nonlinear vibration and dynamic response of functionally graded plates in thermal environments. *Int J Solids Struct* 2004; 41:2403-07.
27. Yuda H, Zhiqiang Z.: Bifurcation and chaos of thin circular functionally graded plate in thermal environment. *Chaos Solitons Fractals* 2011; 44:739–750.
28. Hao YX, Chen LH, Zhang W, Lei JG. Nonlinear oscillations, bifurcations and chaos of functionally graded materials plate. *J Sound Vib* 2008; 312:862-92.
29. Zhang W, Yang J, Hao Y. Chaotic vibrations of an orthotropic FGM rectangular plate based on third-order shear deformation theory. *Nonlinear Dyn* 2010; 59(4):619-60.
30. Warminska A, Manoach E, Warminski J. Dynamics of a circular Mindlin plate under mechanical loading and elevated temperature. In: *MATEC web of conferences* 2016; 83:05013.
31. Manoach E, Warminska A, Warminski J, Doneva S. A reduced multimodal thermoelastic model of a circular Mindlin plate. *Int J Mech Sci* 2019; 153-154: 479-89.
32. Chang WP, Wan SM. Thermomechanically coupled non-linear vibration of plates. *Int J Non-Linear Mech* 1986; 21(5): 375-89.
33. Shu X, Zhang X, Zhang J. Thermoelastic free vibration of clamped circular plate. *Appl Math Mech* 2000; 21(6):715-24.
34. Yeh YL, Chen CK, Lai HY. Chaotic and bifurcation dynamic for a simply supported rectangular plate with thermo-mechanical coupling in large deflection. *Chaos Solitons Fractals* 2002;13:1493-506.
35. Yeh YL. Chaotic and bifurcation dynamic behavior of a simply supported rectangular orthotropic plate with thermo-mechanical coupling. *Chaos Solitons Fractals* 2005; 24(5):1243-55.
36. Yeh YL. The effect of thermo-mechanical coupling for a simply supported orthotropic rectangular plate on non-linear dynamics. *Thin-Walled Struct* 2005; 43(8):1277-95.
37. Robaldo A, Carrera E, Benjeddou A. Unified formulation for finite element thermoelastic analysis of multilayered anisotropic composite plates. *J Therm Stresses* 2005;28(10):1031–65.
38. Fantuzzi N, Tornabene F, Viola E, Ferreira AJM. A strong formulation finite element method (SFEM) based on RBF and GDQ techniques for the static and dynamic analyses of laminated plates of arbitrary shape. *Meccanica* 2014;49:2503–42.
39. Settini V, Saetta E, Rega G. Local and global nonlinear dynamics of thermomechanically coupled laminated plates in passive thermal regime. *Nonlinear Dyn* 2018; 93(1):167-87.
40. Settini V, Rega G, Saetta E. Avoiding/inducing dynamic buckling in a thermomechanically coupled plate: a local and global analysis of slow/fast response. *Proc. R. Soc. A* 2018; 474(2213):20180206-1-24.
41. Settini V, Saetta E, Rega G. Nonlinear dynamics of a third-order reduced model of thermomechanically coupled plate under different thermal excitations. *Meccanica* 2020; DOI: 10.1007/s11012-019-01117-w
42. Saetta E, Rega G. Unified 2D continuous and reduced order modelling of thermomechanically coupled laminated plate for nonlinear vibrations. *Meccanica* 2014; 49(8):1723-49.
43. Saetta E, Rega G. Modelling, dimension reduction, and nonlinear vibrations of thermomechanically coupled laminated plates. *Proc. Eng* 2016; 144:875–882.
44. Saetta E, Rega G. Third-order thermomechanically coupled laminated plates: 2D nonlinear modelling, minimal reduction and transient/post-buckled dynamics under different thermal excitations. *Compos Struct* 2017; 174: 420-441.
45. Saetta E, Settini V, Rega G. Minimal thermal modelling of two-way thermomechanically coupled plates for nonlinear dynamics investigation. *J Therm Stresses* 2020; 43(3):345-71.
46. Settini V, Rega G. Thermomechanical coupling and transient to steady global dynamics of orthotropic plates. In (Eds I Andrianov, A Manevich, Y Mikhlin, O Gendelman) *Problems of Nonlinear Mechanics and Physics of Materials*. Cham: Springer; 2019; *Advanced Structured Materials* 94:483–499.
47. Tonti E. On the mathematical structure of a large class of physical theories. *Rend. Acc. Lincei* 1972; LII:48-56.
48. Tonti E. *The mathematical structure of classical and relativistic physics*. New York: Birkhauser-Springer; 2013.
49. Reddy JN. *Mechanics of laminated composite plates and shells*. Boca Raton: CRC Press; 2004.
50. Pai PF, Nayfeh AH. A nonlinear composite plate theory. *Nonlinear Dyn* 1991; 2:445-77.
51. Nayfeh AH, Pai PF. *Linear and nonlinear structural mechanics*. New York: Wiley; 2004.
52. Rega G, Saetta E. Nonlinear curvature-based model and resonant finite-amplitude vibrations of symmetric cross-ply laminates. *J. Sound Vibration* 2012; 331:2836–55.
53. Rega G, Saetta E. Shear deformable composite plates with nonlinear curvatures: modeling and nonlinear vibrations of symmetric laminates. *Arch Appl Mech* 2012; 82(10–11):1627–52.

54. Nowacki W. Dynamic problems of thermoelasticity. Warszawa: PWN-Polish Scientific Publishers; 1975.
55. Brischetto S, Carrera E. Thermomechanical effect in vibration analysis of one-layered and two-layered plates. *Int J Appl Mech* 2011; 3(1):161-185.
56. Ko WL. Thermal buckling analysis of rectangular panels subjected to humped temperature profile heating. NASA Dryden Flight Research Center Edwards, California [report: NASA/TP-2004 212041, H-2539]; 2004.
57. Luikov AV, Analytical heat diffusion theory. New York: Academic Press; 1968.
58. Tungikar VB, Rao KM. Three-dimensional exact solution of thermal stresses in rectangular composite laminate. *Compos Struct* 1994; 27(4):419-30.
59. Doedel E, Oldeman B. AUTO-07p: Continuation and bifurcation software for ordinary differential equations. Montreal: Concordia University Press; 2012.
60. Wolfram Research, Inc., Mathematica, Version 12.0, Champaign, IL; 2019.